Inverse Design of Photonic Structures using Topology Optimization

by

Ayşemine Altındağ

A Dissertation Submitted to the
Graduate School of Sciences and Engineering
in Partial Fulfillment of the Requirements for
the Degree of

Master of Science

in

Electrical and Electronics Engineering

KOÇ ÜNİVERSİTESİ

March 16, 2023

Inverse Design of Photonic Structures using Topology Optimization

Koç University

Graduate School of Sciences and Engineering

This is to certify that I have examined this copy of a master's thesis by

Ayşemine Altındağ

and have found that it is complete and satisfactory in all respects,
and that any and all revisions required by the final
examining committee have been made.

Committee Members:

Asst. Prof. Emir Salih Mağden (Advisor)

Prof. Alper Kiraz

Assoc. Prof. Onur Ferhanoğlu

Date:

dedicated to my parents Nalan Altındağ and Ahmet Altındağ

ABSTRACT

Inverse Design of Photonic Structures using Topology Optimization
Ayşemine Altındağ
Master of Science in Electrical and Electronics Engineering
March 16, 2023

Photonic inverse design methods are significantly more efficient than traditional photonic design methods. Unlike traditional methods, it operates on the full design area with only two simulations, forward and adjoint simulations.

Using the topology optimization method in the inverse design of photonic devices enables the devices to be optimized for user-specified parameters. The topology optimization method shows better performance when compared to other methods. On the other hand, the fabrication compatibility of device geometries is the most significant challenge with structures created through topology optimization.

In this thesis, fabrication-compatible photonic devices, a power splitter, and a spectral filter are designed using the topology optimization method. To make the devices more fabrication-compatible, filtering methods were used to remove small features and smooth sharp corners. 90%:10% power splitters and spectral filters were fabricated on silicon-on-insulator and devices exhibited sufficient performance.

ÖZETÇE

Fotonik Yapıların Topoloji Optimizasyonu Kullanılarak Ters Tasarımı
Ayşemine Altındağ
Elektrik ve Elektronik Mühendisliği, Yüksek Lisans
16 Mart 2023

Fotonik ters tasarım yöntemleri, geleneksel fotonik tasarım yöntemlerinden oldukça daha verimlidir. Geleneksel yöntemlerin aksine, sadece iki simülasyonla, forward ve adjoint simülasyonlar, tüm tasarım alanı üzerinde işlem yapar.

Fotonik cihazların ters tasarımında topoloji optimizasyon yönteminin kullanılması, cihazların kullanıcı tarafından belirlenen parametreler için optimize edilmesini sağlar. Topoloji optimizasyon yöntemi, diğer yöntemlerle karşılaştırıldığında daha iyi performans göstermektedir. Öte yandan, aygıt geometrilerinin fabrikasyon ile uyumluluğu, topoloji optimizasyonu ile oluşturulan yapılardaki en önemli zorluktur.

Bu tezde, topoloji optimizasyonu yöntemini kullanarak fabrikasyon ile uyumlu fotonik aygıtlar, bir güç ayrıştırıcı ve bir spektral filtre tasarlandı. Aygıtları fabrikasyona daha uyumlu hale getirmek için küçük özellikleri azaltan ve keskin köşeleri yumuşatan filtreleme yöntemleri kullanıldı. 90%:10% güç ayrıştırıcılar ve spektral filtreler yalıtkan üzerine silikon üzerinde üretildi ve cihazlar başarılı performans sergiledi.

ACKNOWLEDGMENTS

I would like to thank my advisor Asst. Prof Emir Salih Mağden for his encouragement, contribution, support, and guidance. Working with him improved me not only in silicon photonics, integrated photonics design, and research experience but also in communication, teamwork, organization, and discipline. I am grateful to him for the opportunity to work with him and to work at Photonic Architecture Laboratories. I would also like to thank committee members Prof. Alper Kiraz and Assoc. Prof. Onur Ferhanoğlu.

I would like to acknowledge the Scientific and Technological Research Council of Turkey (TÜBİTAK) for their financial support during my studies.

I would also like to thank all my mates in the PAL group for the time we spent together and for their support. I especially want to thank Onur and Ali for their support, guidance, and pleasant time we spent.

I also owe a debt of gratitude to my friends Ekin, Semih, Elif, Sıla, Gökçe, Arda, and Murat for always supporting me and listening to me. Last but not least, I would like to express my eternal gratitude to my family. Their constant encouragement and belief in me made it possible to complete this thesis.

TABLE OF CONTENTS

LIST OF FIGURES

LIST OF AlgorithmS

ABBREVIATIONS

SiPh	Silicon Photonics
CMOS	Complementary Metal-Oxide-Semiconductor
FDTD	Finite Difference Time Domain
varFDTD	2.5D variational FDTD
FDFD	Finite Difference Frequency Domain
IC	Integrated Circuit
PIC	Photonic Integrated Circuit
2D	Two Dimensional
3D	Three Dimensional
FOM	Figure of Merit
DRC	Design Rule Checking

Chapter 1

INTRODUCTION

This chapter covers developments and concepts of silicon photonics, photonics design, and the organization of the thesis.

1.1 Silicon Photonics

The development of electronic systems and integrated electronic circuits plays a significant role in the advancement of silicon photonics. The electronic revolution started with the invention of the transistor. Transistors enable to implementation of integrated circuits and microprocessors throughout the years. They have inside of thousands of transistors that are grouped to manage different tasks. This technological leap led to the creation and development of today's CMOS technology. CMOS technology is used to fabricate integrated circuits and enables us to do tasks in a much more scalable manner. Silicon is used as a material in electronic integrated circuits because of its many advantages. It is used with CMOS technology as well. Silicon on insulator CMOS technology enables integrated circuits to perform at high temperatures and reduces capacitance, allowing circuits to operate quickly and with low power. It also reduces noise.

Silicon photonics(SiPh) is simply using silicon as the material for photonic devices. The fundamental advantages of silicon photonics are that silicon is compatible with existing electronic IC fabrication methods and is a cheap and high-quality material. A further significant advantage is that due to the high index contrast between silicon and silicon dioxide, extremely low insertion loss. The confinement in the waveguide is high, and the light propagates inside the waveguide without or with extremely low leakage because of the high index contrast, so they feature low insertion loss [Wong et al., 2007]. This enables photonic devices to be designed in smaller sizes (nano-level). Silicon-based platforms can be used to design photonic devices of any desired geometry and are applicable for both large-scale and small-scale structures. The large index contrast also enables the detection of nonlinear optical interactions [Jalali and Fathpour, 2006]. The thermo-optic and electro-optic characteristics of silicon also make silicon photonics efficient and advantageous. Silicone's high thermal conductivity, high optical damage threshold, and high third-order nonlinear optical properties are highly beneficial for photonic systems[Jalali and Fathpour, 2006]. Achieving highly efficient devices, and robust simulation results are the other benefits of silicon-based platforms.

Important applications of silicon photonics are optical communications, sensor applications, biosensor systems, and spectroscopy. Passive devices, detectors, optical amplifiers, and lasers are examples of significant silicon photonic devices.

1.2 Photonic Design

Photonic design is the process of specifying the physical design parameters to obtain the device geometry that best corresponds to the desired device properties and functions. Photonic design can be considered an optimization problem. And electromagnetic simulations are performed for the specified design parameters and device properties until the desired result is achieved.

The photonic design optimization problem can be solved using heuristic optimization [Angeris et al., 2021] methods such as particle swarm optimization method [Zhang et al., 2013], and genetic optimization [Sanchis et al., 2009] method. However, the Maxwell equations solved during optimization are computationally difficult to solve, so the computational cost for these operations is high. Therefore, heuristic optimization methods are effective for the optimization of photonic devices with simple geometric structures, but they are not efficient and effective for devices with complex structures.

In traditional photonic design methods, photonic devices are designed by the designer using photonic components with specific functional and material properties by specifying the device structure and properties such as length, thickness, and radius as shown in Figure 1.1.

Figure 1.1: (a) Initial guess for straight waveguide for specific functionality, (b) Initial guess for ring resonator, (c) Initial guess for 50%:50% power splitter

Using these photonic devices and components and combining photonic designs, other photonic devices with different and complex functionalities can be designed. The traditional photonic design practice is efficient, but time-consuming and requires a lot of detailed consideration and processing. In addition, the device design may not achieve the desired physical and functional properties [Angeris et al., 2021]. Besides, traditional methods can be used in the design of photonic devices with simple geometrical structures. Therefore, heuristic optimization methods are often effective for traditional methods. Figure 1.2 below shows photonic devices designed with photonic design libraries. As can clearly be observed, they have very simple geometrical structures.

On the other hand, photonic devices with more complex functions and geometrical structures can be designed using the adjoint-based inverse design method. The inverse design method is basically obtaining the device geometry by determining the desired electromagnetic outputs. Unlike other optimization methods, the adjoint optimization method solves the optimization problems for all design parameters by performing only two simulations instead of performing simulations for each

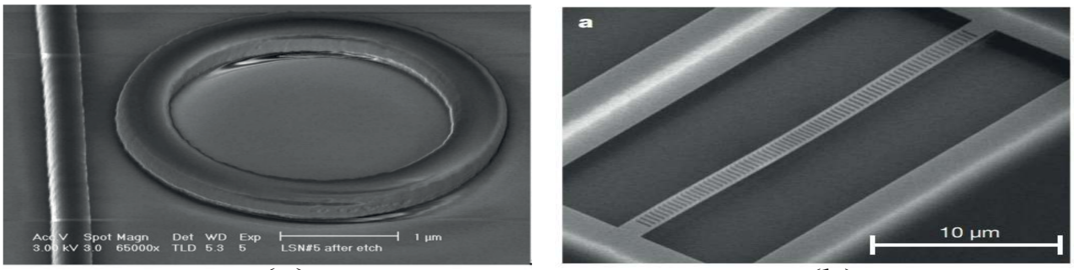

(a) (b)

Figure 1.2: (a) Ring resonator [Xu et al., 2008], (b) Optomechanical crystal [Eichenfield et al., 2009]

parameter. Therefore, it is faster and more efficient than other methods.

In this thesis, photonic device design using an adjoint-based inverse design method is described.

1.3 Organization

The organization of the following parts is as follows: In chapter 2, inverse design methods in photonics design, and topology optimization, and adjoint optimization methods are covered, design and simulation results of photonic components using inverse design are represented in chapter 3. Next, we present the fabrication processes and measurement results of these photonic devices in chapter 4. We conclude in chapter 5 with some remarks and future directions.

Chapter 2

INVERSE DESIGN

Photonic integrated circuits are one of the most important elements that meet the needs of diverse applications, especially communication systems, which are becoming increasingly important today. Basically, photonic devices are used to create, detect and manipulate light. Photonic devices can have various functions such as transferring data through optical signals, multiplexing, and demultiplexing wavelengths, and converting optical data to electrical signals and displays. The wide range of functions and their applicability in different fields make photonic integrated circuits more functional, effective, and attractive. Therefore, more efficiency and increased tolerance for fabrication constraints are required for individual photonic components. These requirements make photonic components and devices more complex. To design more compact, efficient, and fabrication-compatible photonic devices, a new design method was needed other than traditional design methods.

The inverse design method is occurred to find an answer to what should be the geometry for desired performance [Miller, 2012]. The objective of the inverse design method is to determine the device structure that gives the desired electromagnetic results and maximizes the performance goals without violating any constraints defined in the optimization. Inverse design methods make it possible to perform design by determining fabrication and design constraints, and performance goals such as minimizing loss, maximizing transmission, and splitting power with different ratios. [OPTICA, 2022].

Like other photonic design methods, inverse design methods start with solving Maxwell's equation using FDTD, FDFD and etc. The inverse design problem is a mathematical optimization problem solved by rewriting Maxwell's equations(Equation 2.1). And the wavelengths at which the optimization is solved and all calculated electromagnetic fields are solutions of these equations [Miller, 2012]

[Yin, 2019].

Maxwell's equations:

$$\begin{aligned} \nabla \cdot \epsilon \mathbf{E} &= \rho \\ \nabla \cdot \mu \mathbf{H} &= 0 \\ \nabla \times \mathbf{E} &= -j\omega\mu\mathbf{H} \\ \nabla \times \mathbf{H} &= \mathbf{J} + j\omega\epsilon\mathbf{E} \end{aligned} \tag{2.1}$$

Two problems, which are forward and inverse problems, are solved during the inverse design process. In Figure 2.1, the inverse design optimization flow is shown. The forward simulation finds electric and magnetic fields for a given geometry easily. However, it is not easy to solve the inverse problem. Therefore, several optimization methods have been used to solve the inverse problem. In this work, the inverse design of photonic devices is performed using an adjoint-based topology optimization method.

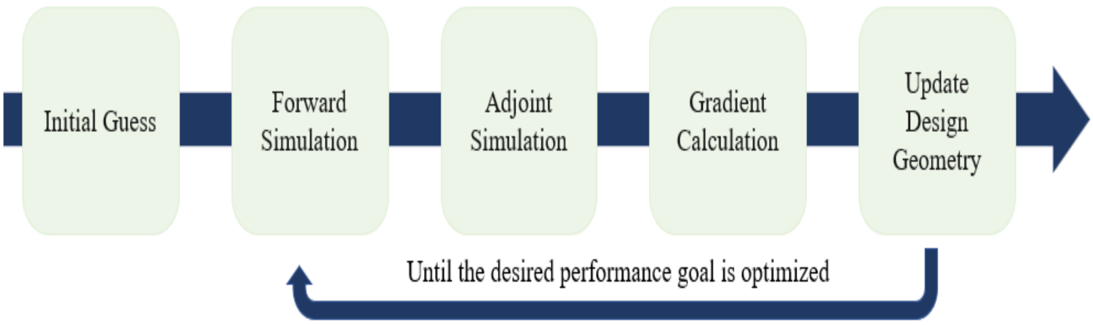

Figure 2.1: Steps of Inverse Design Method

This inverse design process is based on the adjoint shape optimization method. The adjoint method calculates shape derivatives for each point using two simulations: forward and adjoint simulation [Lalau-Keraly et al., 2013].

At the beginning of optimization, an arbitrary initial guess is determined. First, the forward problem is solved using FDTD, and forward electric and magnetic fields are found. The forward simulation also calculates the objective function value. After solving the forward problem, the inverse problem is solved to find adjoint electric and magnetic fields. Then, optimization calculates gradients using forward and adjoint fields. Using calculated gradients and design variables, device geometry is updated as the last step of each iteration of the optimization. These processes continue until the desired objective function values are obtained.

The following Figure 2.2 shows the device geometries at various iterations through the inverse design process of the photonic device, from the initial guess to the final optimized device.

(a) (b) (c) (d) (e)

Figure 2.2: Design of the photonic device at various iterations of optimization

2.1 Topology Optimization Method

Although the topology optimization method was first developed for mechanical design problems, it has been widely used in the design of photonic devices [Jensen and Sigmund, 2011]. It is more efficient and effective than other optimization methods. To perform inverse design using shape optimization, device geometry is parameterized. However, the topology optimization method is performed without parameterizing the geometry, it is sufficient to specify the design space to be optimized.

Using topology optimization for the inverse design of photonic systems enables designers to design by specifying just performance targets and design variables. Photonic devices, components, and systems designed using the topology optimization method successfully achieve the performance and structural targets specified by the designer. The topology optimization method does not have any design limit or restriction. Topology optimization first allows any material between low and high permittivity (Figure 2.3) and smooths design geometry, then it starts gradually to push material to low or high permittivity values (Figure 2.2). Depending on the initial guess used, any geometric structure can be obtained at the end of the optimization. By changing the initial guess, devices with different geometric structures with the same functionality are obtained. That is, it is the initial guess used in the optimization that makes the device design unique.

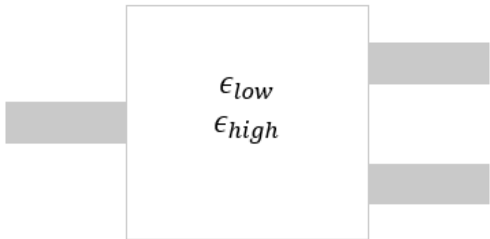

Figure 2.3

Figure 2.4 below shows how topology optimization parametrizes the device design. By binarizing the design variables, 0 and 1 for materials are used in the design, and optimization is performed.

Topology optimization calculations are basic gradient calculations of each point in the design region with respect to the design region. The gradient calculations are quite time-consuming in the inverse design process, so it is necessary to do these calculations as wisely as possible. To perform gradient calculations faster and more efficiently, the adjoint optimization method is used in the topology optimization method[Christiansen and Sigmund, 2021].

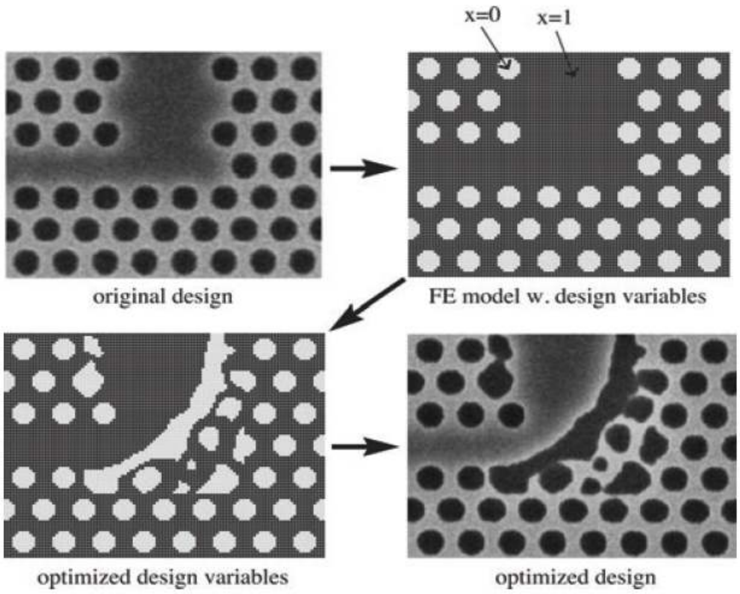

Figure 2.4: Parametrization of the photonic device design during topology optimization [Jensen and Sigmund, 2011]

2.2 *Adjoint Shape Optimization Method*

The main challenge in the design of photonic systems is the optimization of devices with the desired performance. Since the computational cost of the calculations performed during the optimization of the photonic device can be high, so optimizations can take a long time and the convergence is slow. Moreover, the convergence of the optimization of complex devices is even slower. To overcome this significant challenge, the inverse design problem should be solved using gradient-based algorithms like the adjoint shape optimization method. Hence, to achieve high computational efficiency and fast optimization convergence, optimization methods such as topology and shape optimization are based on the adjoint shape optimization method[Yeung et al., 2022].

The adjoint shape optimization method is fast and efficient optimization. By solving only two simulations, forward and adjoint simulations, it calculates the shape derivative for all points in the design region[Lalau-Keraly et al., 2013]. The forward simulation calculates the objective function value, then the adjoint simulation calculates the gradient of the objective function. That is, the adjoint shape optimization calculates the gradient using the forward and adjoint fields. Forward and adjoint simulation and gradient calculation are performed at each iteration of the optimization. The adjoint method reaches the optimum result by changing the device geometry using the gradients calculated in each iteration of the optimization.

The mathematical operations of adjoint optimization can be expressed as follows.

$$\begin{aligned} \nabla \times \vec{E} - j\omega\mu\vec{H} &= \vec{M} \\ \nabla \times \vec{H} + j\omega\epsilon\vec{E} &= \vec{J} \end{aligned} \tag{2.2}$$

Equation 2.2 can be written as Equation 2.3:

$$\mathbf{A}\vec{x} = \vec{b} \tag{2.3}$$

where A $= \begin{bmatrix} j\omega\epsilon(\vec{r}) & \nabla\times \\ \nabla\times & -j\omega\mu(\vec{r}) \end{bmatrix}$, $\vec{x} = \begin{bmatrix} \vec{E} \\ \vec{H} \end{bmatrix}$, and $\vec{b} = \begin{bmatrix} \vec{J} \\ \vec{M} \end{bmatrix}$

$$\begin{aligned} \vec{\nabla}_p F &= \left[\frac{\partial F}{\partial p_1}, \frac{\partial F}{\partial p_2}, ..., \frac{\partial F}{\partial p_N}\right] \\ \frac{\partial F}{\partial p_i} &= 2\mathbf{Re}\left\{\frac{\partial F}{\partial \vec{x}}\frac{\vec{x}}{\partial p_i}\right\} \end{aligned} \tag{2.4}$$

$\frac{\partial F}{\partial \vec{x}}$ is already known. Differentiate Equation 2.3:

$$\frac{\partial \mathbf{A}\vec{x}}{\partial p_i} = \frac{\vec{b}}{\partial p_i} \tag{2.5}$$

Equation 2.5 can be written as:

$$\mathbf{A}\frac{\partial \vec{x}}{\partial p_i} = \frac{\vec{b}}{\partial p_i} - \frac{\partial \mathbf{A}}{\partial p_i}\vec{x} \tag{2.6}$$

$$\frac{\partial \vec{x}}{\partial p_i} = \mathbf{A}^{-1}\left(\frac{\vec{b}}{\partial p_i} - \frac{\partial \mathbf{A}}{\partial p_i}\vec{x}\right) \tag{2.7}$$

Since $\frac{\vec{b}}{\partial p_i} = 0$, Equation 2.7 becomes:

$$\frac{\partial \vec{x}}{\partial p_i} = -\mathbf{A}^{-1}\frac{\partial \mathbf{A}}{\partial p_i}\vec{x} \tag{2.8}$$

Back to Equation 2.4:

$$\frac{\partial F}{\partial p_i} = -2\mathbf{Re}\left\{\frac{\partial F}{\partial \vec{x}}\mathbf{A}^{-1}\frac{\partial \mathbf{A}}{\partial p_i}\vec{x}\right\} \tag{2.9}$$

Let's define $y^T = \frac{\partial F}{\partial \vec{x}}\mathbf{A}^{-1}$ where $\vec{y}$ is adjoint field.

$$\mathbf{A}^T\vec{y} = \left(\frac{\partial F}{\partial \vec{x}}\right)^T \tag{2.10}$$

and Equation 2.9 can be written as follow:

$$\frac{\partial F}{\partial p_i} = -2\mathbf{Re}\left\{y^T\frac{\partial \mathbf{A}}{\partial p_i}\vec{x}\right\} \tag{2.11}$$

Chapter 3

INVERSE DESIGN OF PHOTONIC DEVICES

In this chapter, the design of photonic power splitters and spectral filters using the inverse design method is represented. The motivation of the research was to design photonic devices that are more efficient, fabrication-tolerant, and low-loss using the inverse design method and decreasing design optimization time. During the inverse design process, the topology optimization method is used. Inverse design using topology optimization allows optimization to perform and design automatically for design parameters and performance goals which is specified by users.

Lumerical [Lumerical, 2022b] and Meep [MEEP, 2022] are used as photonic simulation tools during the design and optimization of photonic devices. Forward and adjoint simulations are performed using an FDTD solver(Figure 3.1a and Figure 3.1b). FDTD simulations solve Maxwell's equations. FDTD solver is fast and robust, it also performs broadband simulations easily.

During the design process, both two and three-dimensional FDTD simulations can be used. 2D simulations are faster, but 3D simulation results are more accurate, and robust. Therefore, for devices with simpler functions, it is advantageous to use 2D simulations, whereas for more complex structures we can achieve more robust results with 3D simulations. Since 2D simulations can provide more robust results in the design of simple devices, such as 50%:50% splitter, and mode converter, it is more advantageous to use 2D FDTD in the design of these devices. However, to analyze the progress and convergence of the optimization for user-defined design parameters, using 2D simulations for trials may be helpful for 3D design processes.

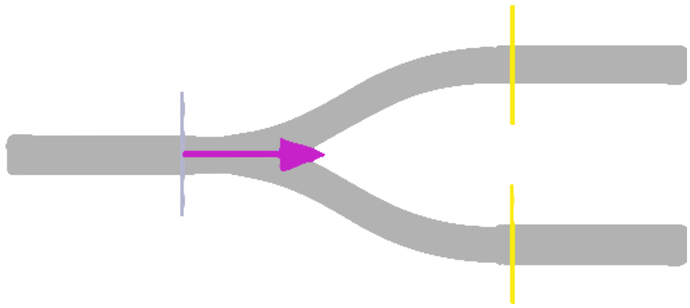

(a)

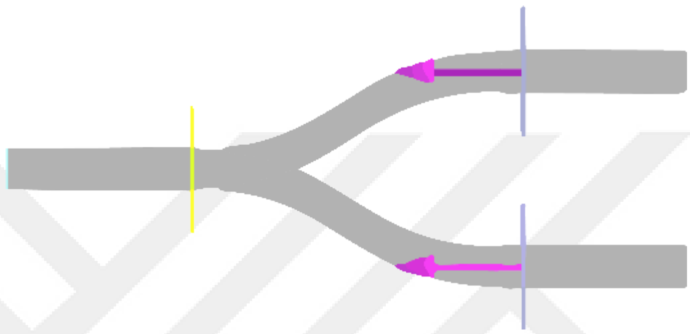

(b)

Figure 3.1: FDTD simulations: (a) Forward Simulation, (b) Adjoint Simulation.

3.1 *Inverse Design of Photonic Splitter*

Photonic power splitters are one of the most important and fundamental components in photonic integrated circuits. Power splitters divide input light power into output waveguides in specified proportions. In general, power splitter designs are quite easy because their functions are simpler compared to other photonic systems, such as the 50%:50% power splitter [Chang et al., 2018] [Xu et al., 2022], which is why they are widely used. Since the power ratio required from the output ports of the 50%:50% power splitter is equal, these power splitters have a symmetrical geometrical structure. Optimization can be performed only to obtain half of the photonic device geometry and then it is possible to combine it with the symmetrical one to obtain the device itself. Therefore, the computational cost of designing a 50%:50% power splitter is low. Since designing photonic devices with different split ratios can be challenging, it is possible to see mostly 50%:50% power splitter examples in previous inverse design studies. Therefore, in my studies, I focused on designing power splitters with different split ratios other than 50%:50% using the inverse design method.

To design a power splitter, lumopt [Lalau-Keraly et al., 2013] [Christopher Lalau-Keraly, 2022], which is an adjoint optimization tool for Lumerical, is used. The inverse design optimization proceeds by solving forward and adjoint problems for each iteration using the L-BFGS-B method[Zhu et al., 1997]. I designed a 90%:10% power splitter using inverse design and topology optimization methods. The function of the 90%:10% power splitter is dividing input power into output ports in 90% and 10%. 90%:10% power splitter is optimized for a 1500-1600 nm wavelength range(center wavelength of 1550 nm) and TE-polarized light.

Fabrication of the photonic devices is the main issue in devices that is designed using topology optimization. To overcome this important challenge, lumopt uses filters to minimize small features and smooth sharp angles. The radius of the filter is defined by a user, so by changing the filter radius, different fabrication constraints can be satisfied.

3.1.1 2D Optimization of 90%:10% Power Splitter

First, a 2D FDTD solver is used to design a power splitter, because 2D simulations are much faster. Material indices are defined as 2.88 (effective refractive index for Si) for the Silicon waveguide and 1.44 for SiO_2 cladding respectively for 2D designs. I determined an initial guess of the Y-shape that Lumerical uses in their inverse design examples, thinking that this Y-shape would be a good start for a 1 x 2 splitter and that the optimization would converge faster. By changing design parameters such as design region area and filter radius, I tried to obtain the most optimum devices that satisfy the required performance goals and fabrication constraints. The optimized 90%:10% splitters with different design region sizes and filter radii are shown in Figure 3.2 and Figure 3.5.

In order to examine the accuracy of the optimized devices with the experimental results, 3D FDTD and varFDTD [Lumerical, 2022c], [Hammer and Ivanova, 2009], simulations of the optimized splitter were performed and compared with the 2D FDTD simulation results. Since varFDTD is faster than 3D FDTD, it was done first, and compared with the 2D FDTD simulation results in Figures 3.3 and 3.6. The simulation results were consistent for both output ports.

Figure 3.2: 90%:10% power splitter with design region area of 6.0 x 6.0 µm^2 and filter radius of 1.0 µm: (a) Initial guess geometry, (b) 90%:10% power splitter.

Based on these results, I decided that the devices could be suitable for fabrication and performed 3D FDTD simulations of the devices shown in Figures 3.2b and 3.5b to obtain the most realistic transmission results. And transmission results from 2D and 3D FDTD simulations are compared in Figure 3.4 and Figure 3.7 respectively.

According to the 3D simulation results of the device with a 6.0 x 6.0 µm^2 design region (Figures 3.2b), the lowest transmission result at the top port is 0.65 (Figure 3.3b) and the lowest transmission result at the bottom port is 0.024 (Figure 3.3c). These results are quite different from the targeted FOM values and indicate that the device will not perform as specified. On the other hand, in the 3D simulation results of the device with 6.0 x 5.0 µm^2 design area (Figure 3.4b), the lowest transmission result at the upper port was 0.76 (Figure 3.5b) and the lowest transmission result at the bottom port was 0.056 (Figure 3.5c). Although it performs better than the other device, these results are still quite different from the targeted FOM values and indicate that the device may not perform as specified.

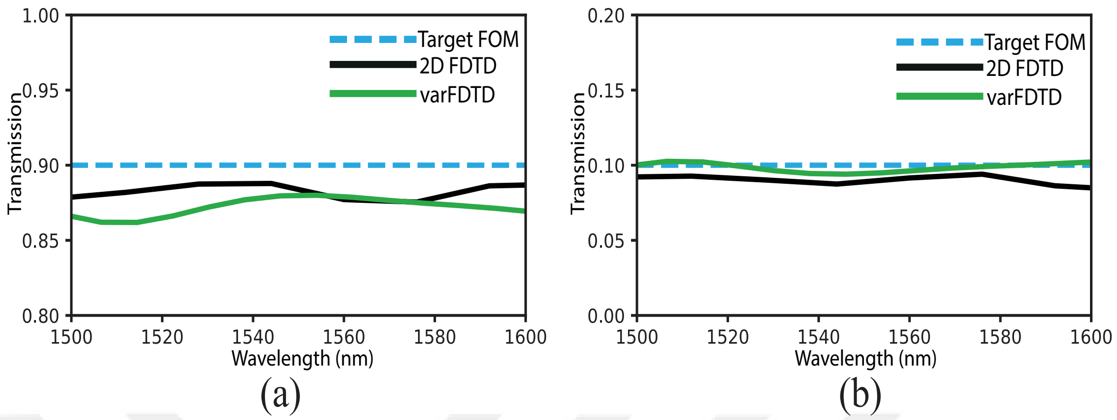

Figure 3.3: Simulation results of 90%:10% power splitter with design region area of 6.0 x 6.0 µm^2 and filter radius of 1.0 µm: (a) 2D FDTD and varFDTD simulation results of the top port, (b) 2D FDTD and varFDTD simulation results of the bottom port.

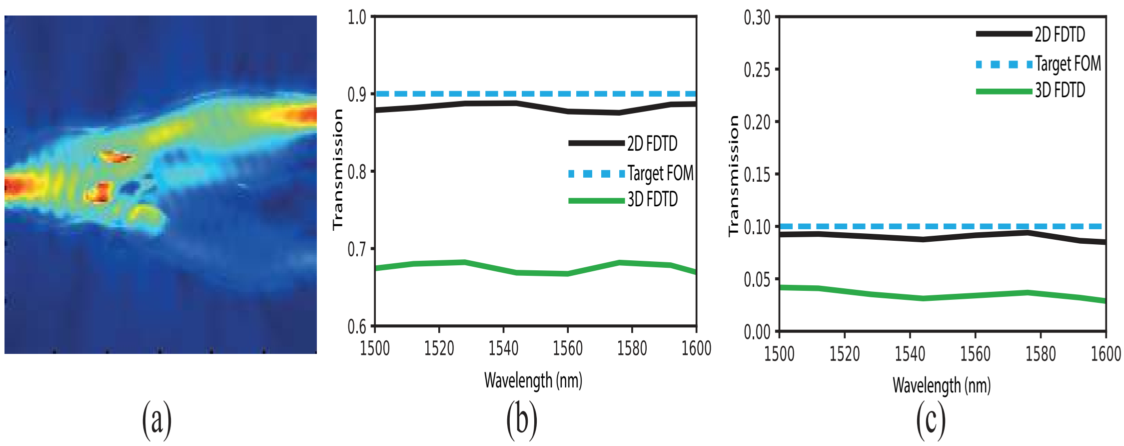

Figure 3.4: Simulation results of 90%:10% power splitter with design region area of 6.0 x 6.0 µm^2 and filter radius of 1.0 µm: (a) Electric field of the 90%:10% power splitter at 1550 nm, (b) 2D and 3D FDTD simulation results of the top port, (c) 2D and 3D FDTD simulation results of the bottom port.

Figure 3.5: 90%:10% power splitter with design region area of 6.0 x 5.0 µm^2 and filter radius of 1.0 µm: (a) Initial guess geometry, (b) Optimized 90%:10% power splitter.

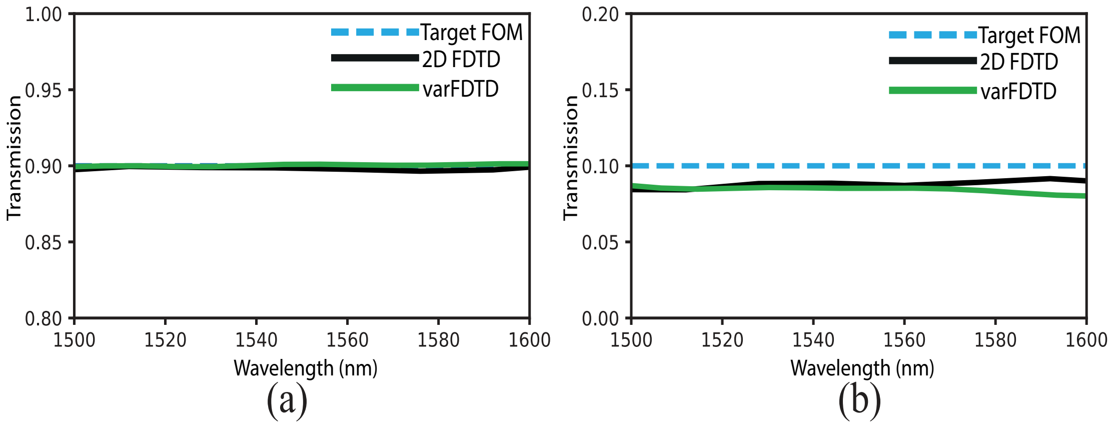

Figure 3.6: Simulation results of 90%:10% power splitter with design region area of 6.0 x 5.0 µm^2 and filter radius of 1.0 µm: (a) 2D FDTD and varFDTD simulation results of the top port, (b) 2D FDTD and varFDTD simulation results of the bottom port.

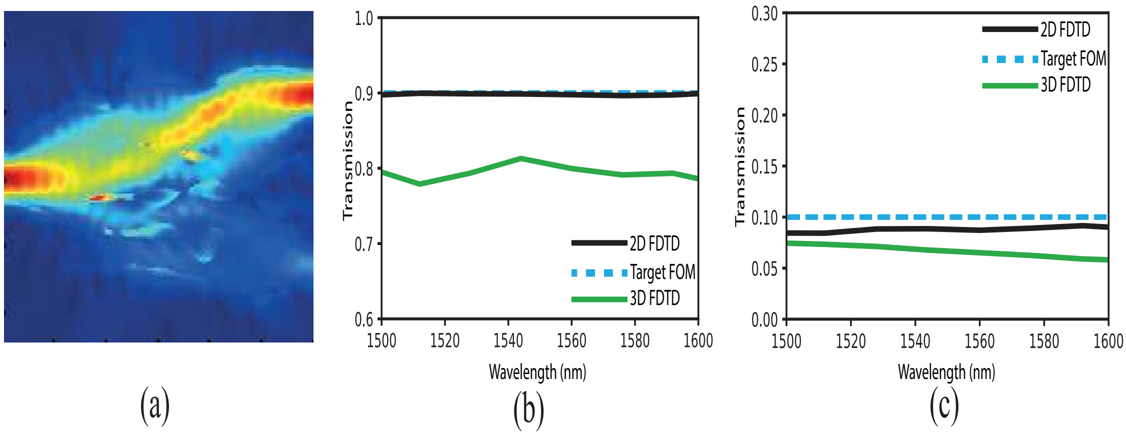

Figure 3.7: Simulation results of 90%:10% power splitter with design region area of 6.0 x 5.0 µm^2 and filter radius of 1.0 µm: (a) Electric field of the 90%:10% power splitter at 1550 nm, (b) 2D and 3D FDTD simulation results of the top port, (c) 2D and 3D FDTD simulation results of the bottom port.

Optimized device geometries are not completely fabrication-compatible. Therefore, with minor modifications, the device geometries are made fabrication-compatible. These changes in the device geometry also cause decreases in the transmission results of the devices.

To minimize the differences between 2D and 3D FDTD simulation results and the impact of possible modifications in the device geometry on the transmission results, it seems that performing inverse design of photonic devices using 3D FDTD simulations will lead to better-performing power splitters.

3.1.2 3D Optimization of 90%:10% Power Splitter

For the 3D simulations, material refractive indices are defined as 3.48 and 1.44 for Si and SiO_2 respectively for 3D designs. Refractive indices values were determined according to the center wavelength of 1550 nm. As the initial guess, I used the Y-shape as in the 2D optimization, but I set the width of the top part larger than the width of the bottom part because according to the 2D optimization results, the top part (the part with 90% power ratio) was wider than the bottom part (the part with 10% power ratio). Since the 3D simulation results of the optimized devices obtained with 2D optimizations were insufficient, the size of the design space was increased while performing 3D optimization. Filter radius is also increased to improve fabrication-tolerances of devices. Two power splitters with design areas of 7.0 x 7.0 µm^2 and 8.0 x 6.0 µm^2 are designed using inverse design with 3D FDTD simulations. First, the device with a design area of 7.0 x 7.0 µm^2 and simulation results are shown, then the device with a design area of 8.0 x 6.0 µm^2 and simulation results are shown.

The graphs in Figures 3.8 and 3.13 shows how the FOM for the two output ports of the device change throughout the optimization, i.e. it shows how the optimization converges.

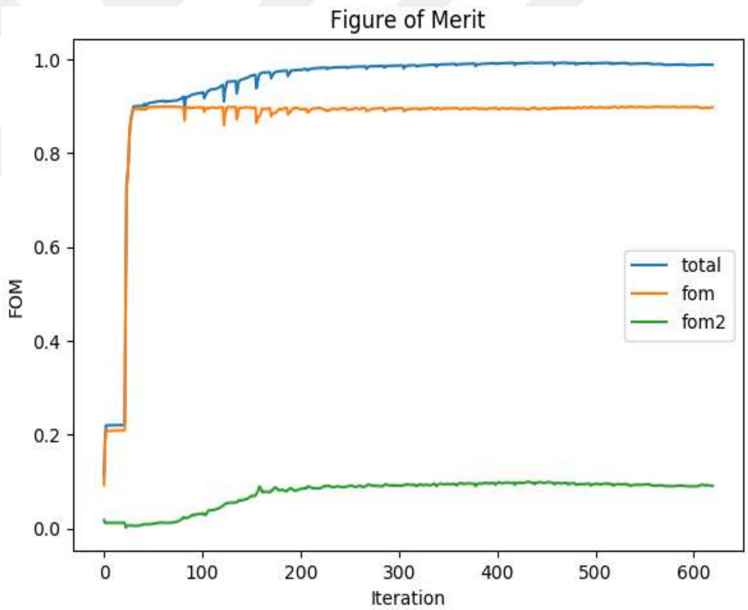

Figure 3.8: Convergence of the optimization of 90%:10% power splitter with design region area of 7.0 x 7.0 µm^2 and filter radius of 1.25 µm

In the following Figures 3.9 and 3.14, the optimized 90%:10% splitters with different design region sizes and filter radii are shown.

The simulated performances of the 3D optimized 90%:10% power splitters (Figure 3.10 and Figure 3.15) match well with the design target and demonstrate broadband and spectrally flat operation over a wavelength range from 1500 to 1600 nm.

Figure 3.9: 90%:10% power splitter with design region area of 7.0 x 7.0 µm^2 and filter radius of 1.25 µm: (a) Initial guess geometry, (b) Optimized 90%:10% power splitter.

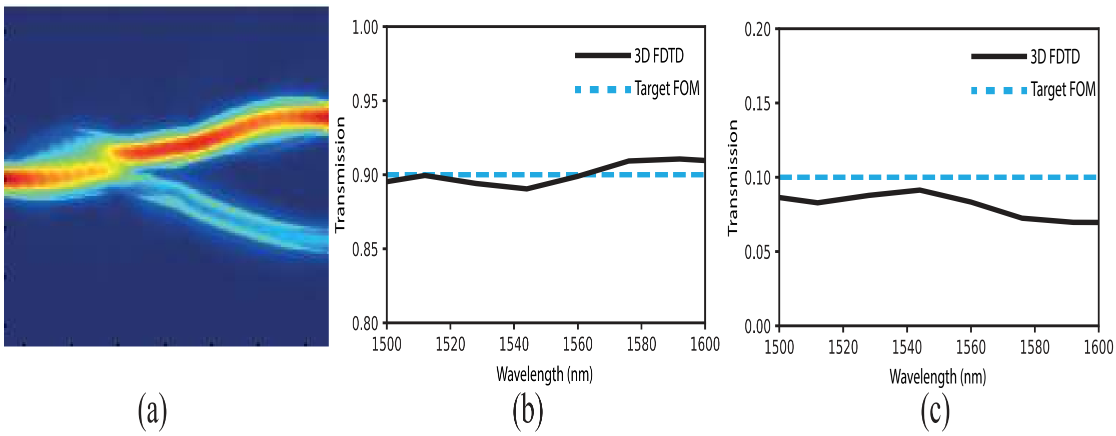

Figure 3.10: Simulation results of 90%:10% power splitter shown in Figure 3.9: (a) Electric field of the 90%:10% power splitter at 1550 nm, (b) 3D FDTD simulation results of the top port, (c) 3D FDTD simulation results of the bottom port.

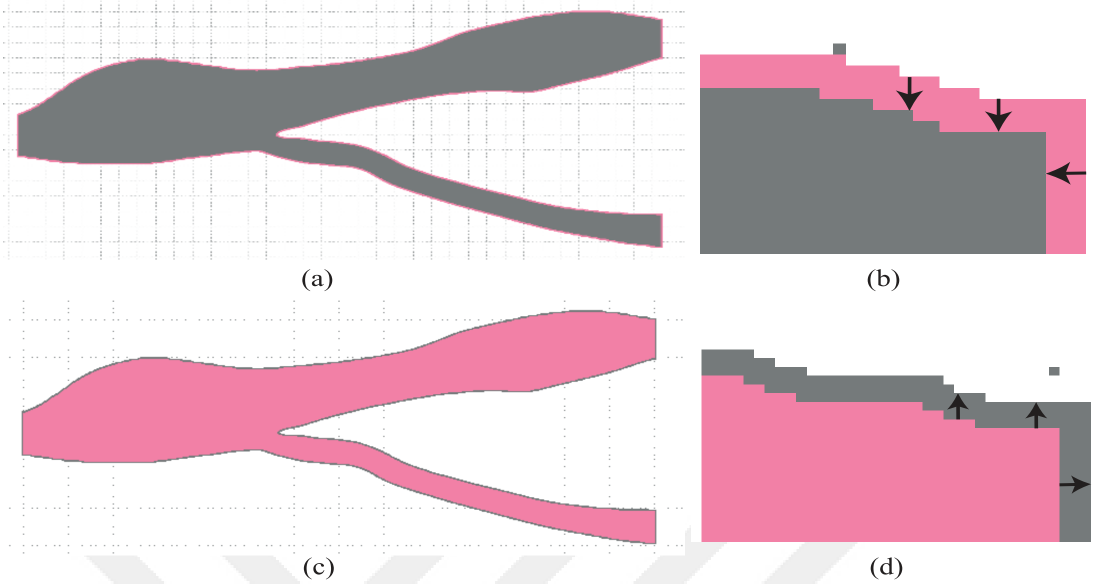

Figure 3.11: Over-etched and under-etched versions of the power splitter shown in Figure 3.9: (a) and (b) Optimized device geometry(pink) and 15 nm over-etched device geometry(gray), (c) and (d) Optimized device geometry(pink) and 15 nm over-etched device geometry(gray).

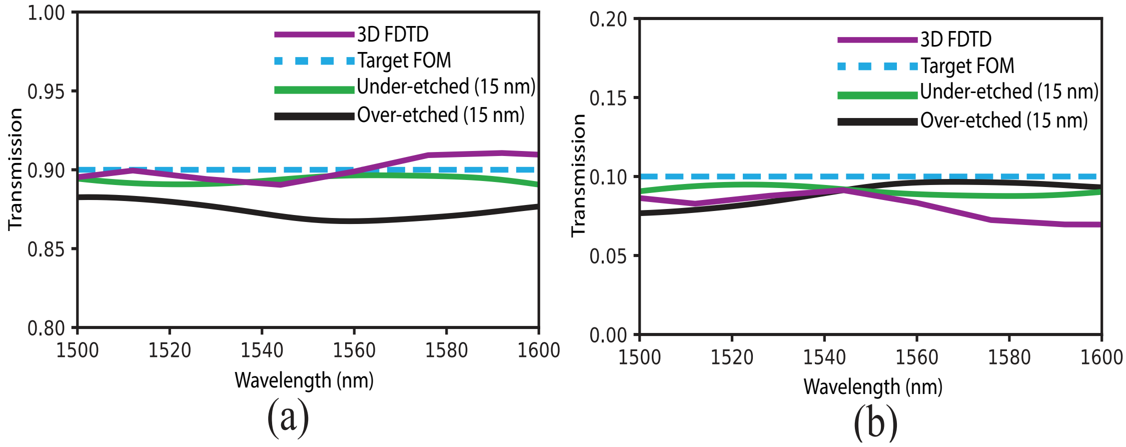

Figure 3.12: Simulation results of 90%:10% power splitter shown in Figure 3.9 and over-etched and under-etched versions of the power splitter: (a) 3D FDTD simulation results of top port for optimized, 15 nm over-etched, and 15 nm under-etched devices, (b) 3D FDTD simulation results of bottom port for optimized, over-etched, and under-etched devices.

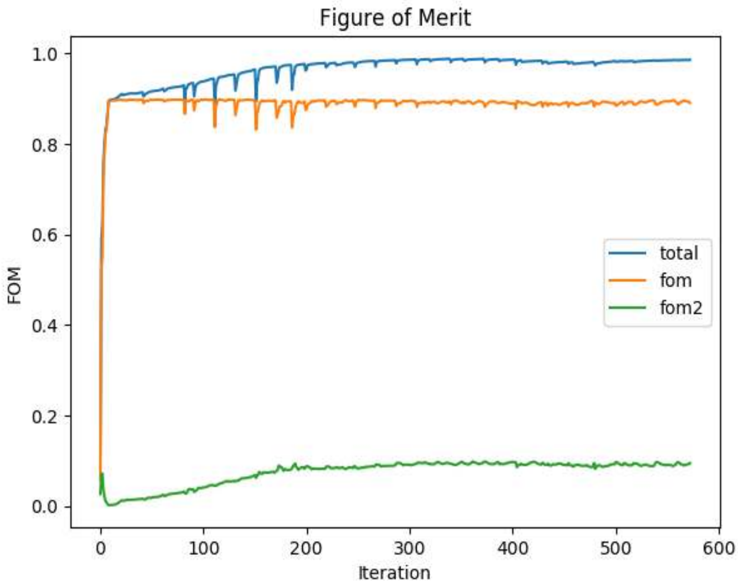

Figure 3.13: Convergence of the optimization for 90%:10% power splitter with design region area of 8.0 x 6.0 μm^2 and filter radius of 1.5 μm

Figure 3.14: 90%:10% power splitter with design region area of 8.0 x 6.0 μm^2 and filter radius of 1.5 μm: (a) Initial guess geometry, (b) Optimized 90%:10% power splitter.

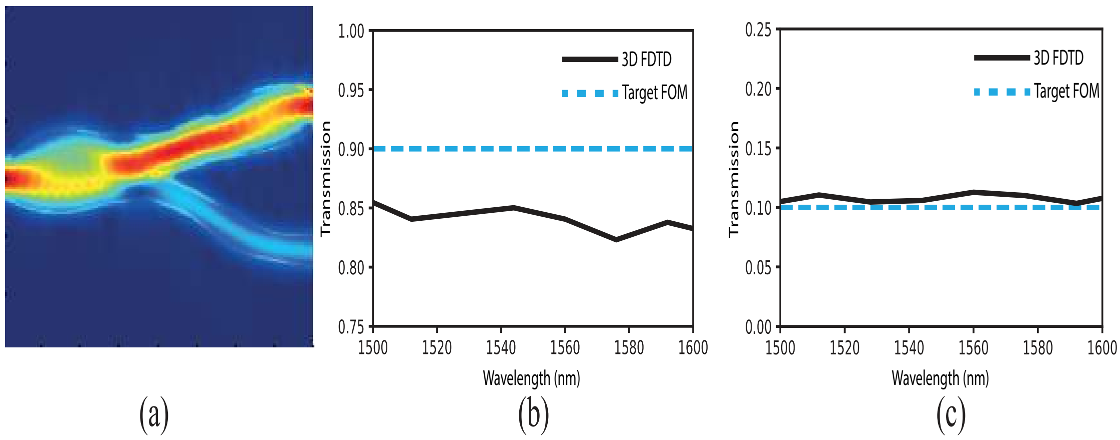

Figure 3.15: Simulation results of 90%:10% power splitter shown in Figure 3.13: (a) Electric field of the 90%:10% power splitter at 1550 nm, (b) 3D FDTD simulation results of the top port, (c) 3D FDTD simulation results of the bottom port.

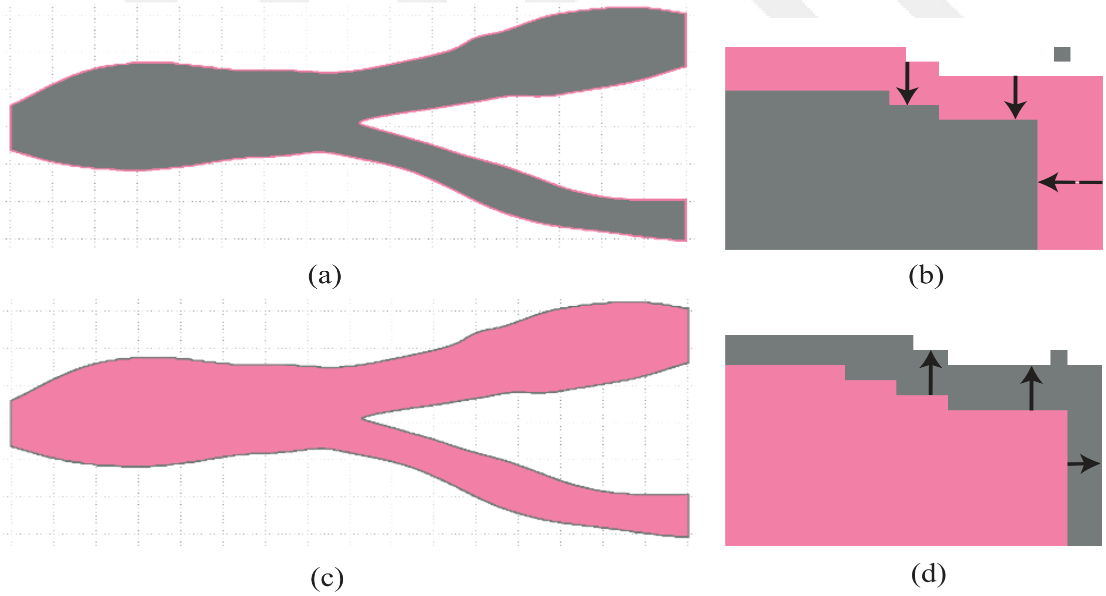

Figure 3.16: Over-etched and under-etched versions of the power splitter shown in Figure 3.14: (a) and (b) Optimized device geometry(pink) and 10 nm over-etched device geometry(gray), (c) and (d) Optimized device geometry(pink) and 10 nm over-etched device geometry(gray).

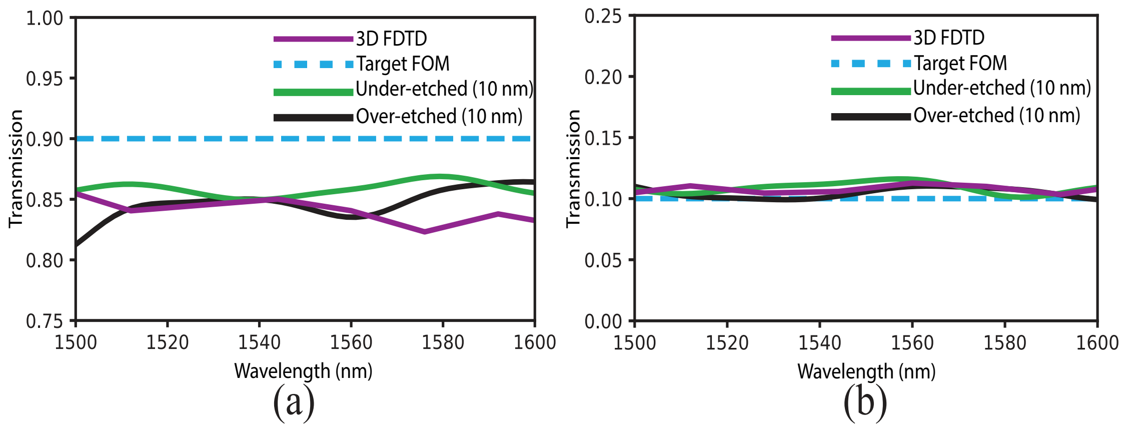

Figure 3.17: Simulation results of 90%:10% power splitter shown in Figure 3.13 and over-etched and under-etched versions of the power splitter: (a) 3D FDTD simulation results of top port for optimized, 10 nm over-etched, and 10 nm under-etched devices, (b) 3D FDTD simulation results of bottom port for optimized, over-etched, and under-etched devices.

Then to verify the designed power splitters' tolerance to potential fabrication changes in device geometry, over-etched (Figure 3.11a and 3.16a) and under-etched(Figure 3.11c and 3.16c) versions of the devices were simulated. Simulation results are shown in Figures 3.12 and 3.17. 3D FDTD results of the modified versions demonstrate minimal change in the transmission of the top and bottom output ports of the device, reaching a maximum deviation of 0.64 dB for the power splitter with a design region size of 7.0 x 7.0 µm^2 and 0.11 dB for the power splitter with a design region size of 8.0 x 6.0 µm^2 (at the center wavelength of 1550 nm) over the original transmission. These simulations verify that these designed devices are fabrication-tolerant.

3.2 Inverse Design of Photonic Spectral Filter

Photonic filters today constitute one of the most important building blocks of silicon photonic systems. They can be used in various fields and applications such as data communication, spectroscopy, image sensors, lasers, fluorescence microscopy[Kalyani and Sharma, 2016], etc.

Photonic spectral filters combine and separate optical signals according to the desired device function. They are used for wavelength multiplexing in many applications. The following Figure 3.18 shows a schematic representation of the filter with upper/lower pass outputs in a 1x2 configuration and its ideal transfer function outputs.

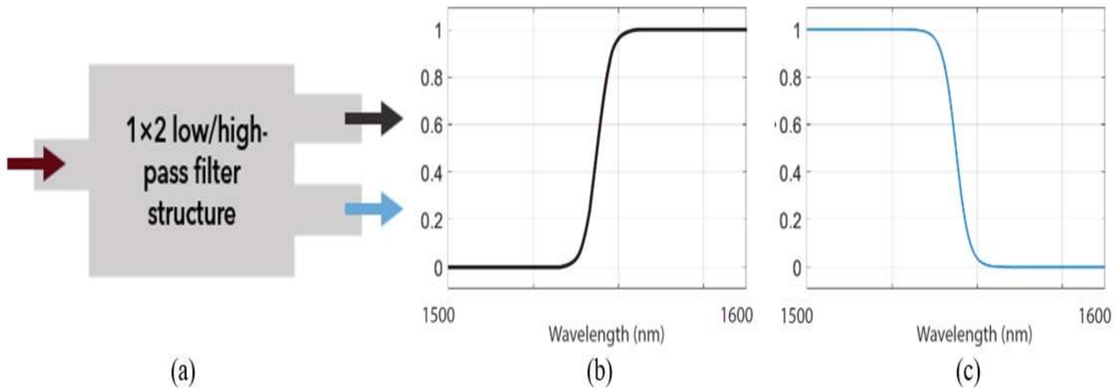

Figure 3.18: (a) Schematic representation of the 1 x 2 filter structure. (b) ideal filter transfer functions for high-pass and (c) low-pass outputs.

Photonic spectral filters often have complex geometric structures. Therefore, their design process is very challenging with traditional methods. It is even possible that the desired photonic spectral filter function cannot be achieved with traditional methods. Designing a spectral filter using the inverse design method is much more efficient and effective than traditional methods. Inverse-designed filters have better performance [Piggott et al., 2016] [Liu et al., 2020] and have smaller footprints.

The functionality of photonic spectral filters is more complex than that of photonic power splitters. The geometrical structures of complex functional devices are also more complex than those of simple photonic devices. Thus, photonic spectral filter design is much more challenging than power splitter design. Optimization takes longer to reach a desired photonic device and the computational cost can be higher. Since photonic spectral filters have more design parameters, the computational cost of gradient calculations is higher.

During the inverse design process of photonic filters using Lumerical, it became clear that the optimization did not converge efficiently, and the optimization would take much longer than the desired, acceptable time due to the slowness of the gradient calculations. Therefore, another electromagnetic simulation tool was used to design the photonic spectral filter. To design a photonic spectral filter, I used Meep as a photonic simulation tool. The adjoint solver tool of Meep is very similar to lumopt, it performs an inverse design method using topology optimization [Hammond et al., 2022]. Optimization computes the objective function value (desired functionality) with forward simulation and its gradient with adjoint simulation for given design parameters.

In the optimization of Meep, a single wavelength range can be defined and the sources for the two output ports for adjoint simulations are created for this specified wavelength range. However, since it is desired to obtain different wavelengths from the outputs of spectral photonic filters, the adjoint sources should be created for different wavelength ranges. Therefore, the adjoint solver tool of Meep is not sufficient for photonic spectral filter design. Hence, we implement our optimization model using the adjoint solver and FDTD solver of Meep. We just modified the adjoint solver tool to design filters. The modifications have been made to the adjoint solver to allow it to perform adjoint simulations for different wavelength ranges specified by the user. The flow of our optimization algorithm is presented below in Algorithm 1.

First, the initial guess geometry and design variables are defined. Then the density values are mapped to the corresponding permittivity values and the specified preprocessor operations are applied to the design. Preprocessor manipulates design variables using smoothing, filtering, projection, opening, and closing operations at each iteration. Therefore, fabrication-compatible photonic devices can be obtained at the end of the optimization process. Then forward simulations are performed. With forward simulations, the objective function is calculated and forward fields are saved. For each forward simulation, adjoint sources are created for specified wavelength ranges and adjoint simulations are performed. In adjoint simulations, adjoint fields are saved and gradient calculations are made and saved as in line 17 in

---

Algorithm 1 Optimization Algorithm for Photonic Spectral Filter Design

---

Define design variables, DV(density values)
while *until convergence* **do**
    Convert DV to PV(permittivity values), Preprocessor
    Convert design variables(PV) to Meep block
    $f_1, f_2, .., f_N$ = [0,0,...,0] (Nx1)
    for $i = 1, 2, \dots, N$ $(for\ each\ forward\ simulation)$ **do**
        Run forward simulation
        Compute and save objective function(f_i)
        Record forward fields
        $\frac{df_i}{d\epsilon} = 0$
        Create adjoint sources
        for ($for\ each\ adjoint\ simulation$) **do**
            Select adjoint source $(x_1, x_2, ..)$
            Run adjoint simulation
            Record adjoint fields
            Calculate gradients
            Accumulate and save $\frac{df_i}{d\epsilon}(1xN)$
        end for
    end for
    Compute F from $[f_1, f_2, .., f_N]$
    $\frac{dF}{d\epsilon} = \sum(\frac{dF}{df_i} * \frac{df_i}{d\epsilon})$ (array summation)
    $\frac{dF}{dPV} = \frac{dF}{d\epsilon} * \frac{d\epsilon}{dPV}$ (Meep backpropagation)
    $\frac{dF}{dDV} = \frac{dF}{dPV} * \frac{dPV}{dDV}$ (Preprocessor backpropagation)
    Update (F, $\frac{dF}{dDV}$, DV)
    return PV
end while

---

the algorithm. And the device geometry is updated using the calculated gradients. The optimization continues until the specified stop conditions, reaching a certain discreteness value or a specified maximum iteration number, are met or the desired objective function value is reached.

In our optimization model, the preprocessor step, the creation of adjoint sources, and the creation of the geometry were implemented differently from Meep. General inverse design operations and steps were performed with existing functions in Meep.

To ensure that the designed devices are fabrication-compatible, penalty filters [Dasdemir et al., 2020] [Christiansen and Sigmund, 2021] [Christiansen et al., 2015] [Zhou et al., 2015] and functions are applied during optimization. Their aim is to reduce small features, sharp angles, and corners in the device structure. When the objective function value reaches the user-specified value or the device structure achieves a user-specified discreteness level, these penalty filters and functions are applied at each iteration. The Gaussian low-pass filter is applied to achieve desired minimum feature size, and a sigmoid-like projection function is applied to control the binarization of the structure. By applying a smoothing filter and binarization projection, fabrication-compatible devices with smooth corners and desired feature sizes are obtained[Dasdemir et al., 2020].

3.2.1 3D Optimization of Photonic Spectral Filter

Since the spectral filter's function is complex I did not apply 2D simulations because the accuracy of 2D simulations for complex structures may not be sufficient. 3D FDTD simulations were used for photonic inverse design optimization of the photonic spectral filter.

Material indices are defined as 3.48 and 1.44 for Si and SiO_2 respectively for 3D designs of photonic spectral filters. I also used two different initial guesses, one is a discrete structure, which is similar to the photonic crystal structure, and the other one is a continuous structure with a permittivity between the permittivities of Si and SiO_2. The input power wavelength range is determined between 1500-1600nm, and the desired wavelength ranges to be received from the outputs were determined as 1500-1550nm and 1560-1600nm.

To design the best optimized photonic spectral filter, various optimizations are performed by changing the design region area, initial guess structure, and filter radius. In the following figures, inverse design optimization results at each iteration, optimized photonic spectral filters, and their simulation results are shown.

Figures 3.19b, 3.22b, and 3.24b show the values of the penalty functions throughout the optimization. Penalty functions start after the optimization has proceeded for a while and some user-specified constraints, such as discreteness of the device geometry and objective function value, have been satisfied. When penalty functions are applied from the first iteration of the optimization, the optimization cannot converge to the desired objective function. The dashed lines in Figures 3.19a, 3.22a, and 3.24a show where the beta value increases. That is, the discreteness of the device geometry increases at these points. The beta values are increased when the objective function error value is below a certain value and the optimization is advanced.

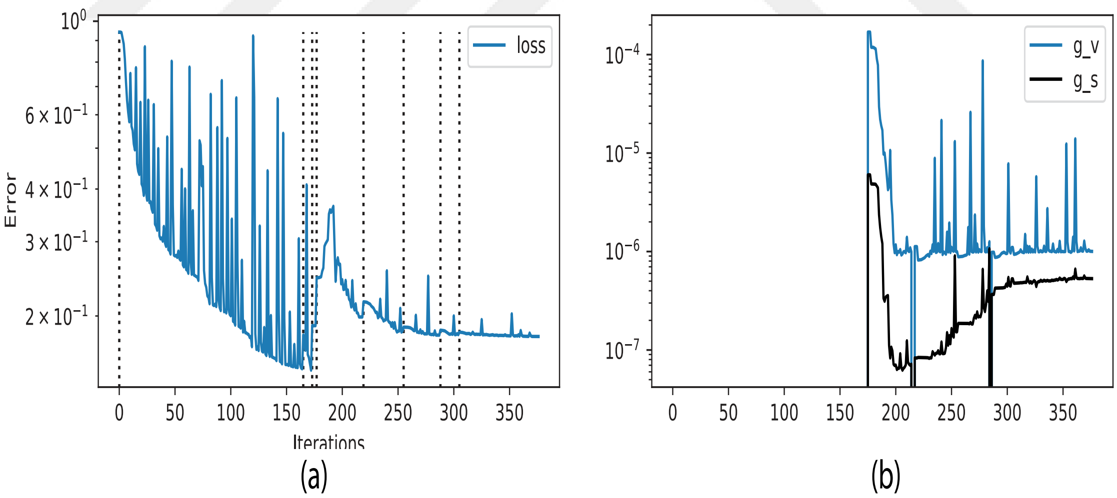

Figure 3.19: Photonic spectral filter with design region area of 5.4 x 6.0 µm², the radius of 100 nm, and penalty radius of 100 nm : (a) Objective function error throughout optimization, (b) Penalty functions throughout optimization

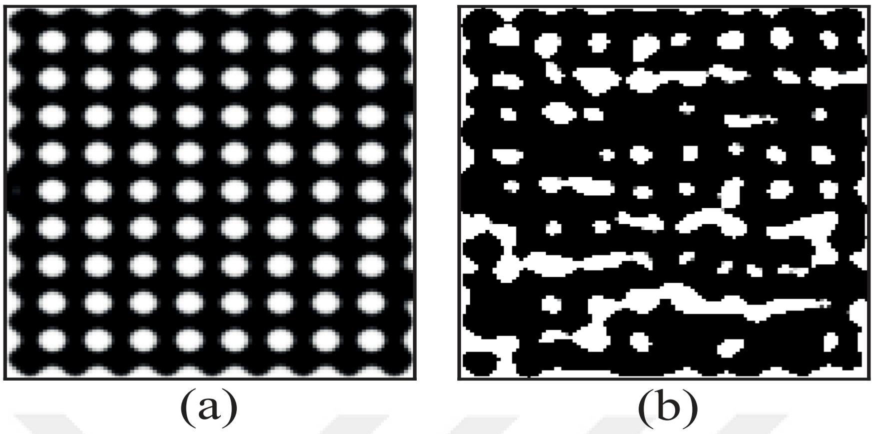

Figure 3.20: Photonic spectral filter with design region area of 5.4 x 6.0 µm^2, the radius of 100 nm, and penalty radius of 100 nm : (a) Initial guess geometry (radius of circles are 200 nm and the gap between circles is 200 nm), (b) Optimized photonic spectral filter.

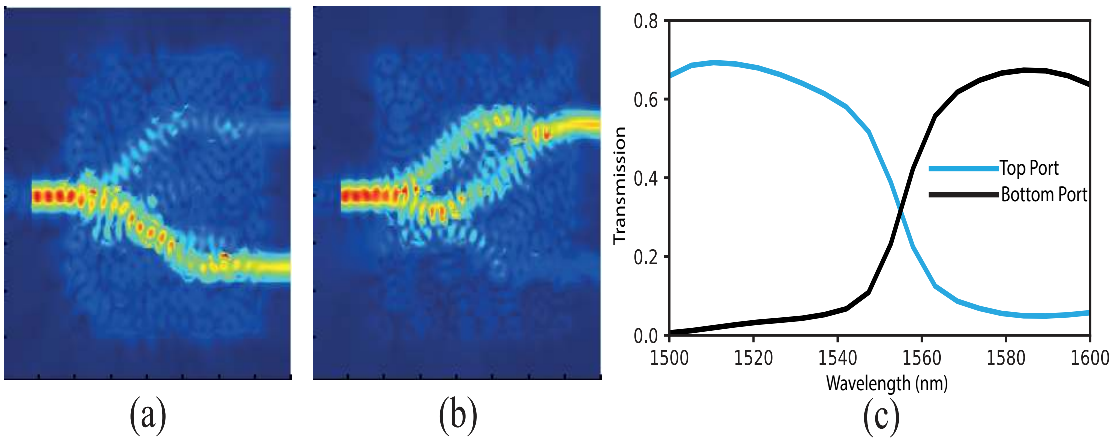

Figure 3.21: Simulation results of the photonic spectral filter shown in Figure 3.20: (a) Electric field at 1590 nm, (b) Electric field at 1510 nm, (c) 3D FDTD simulation results.

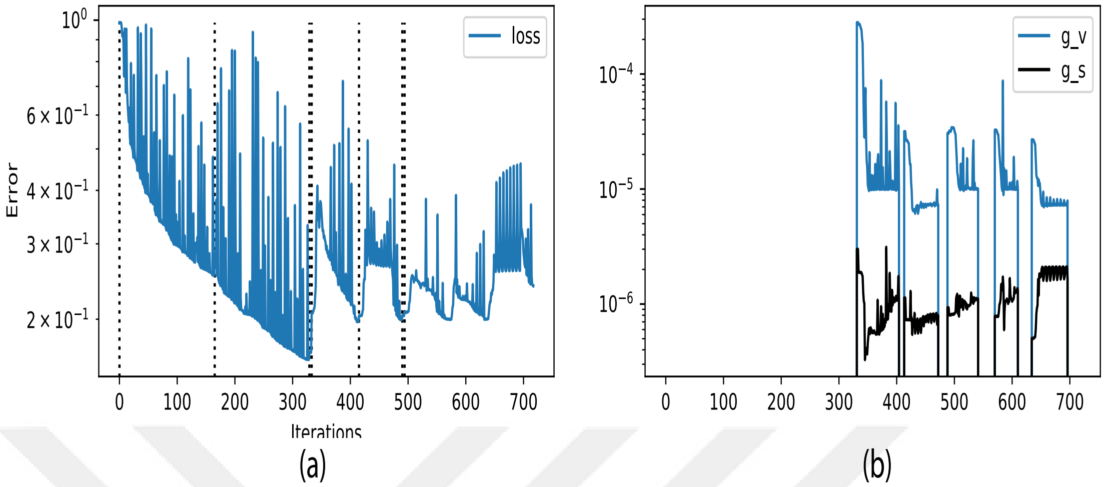

Figure 3.22: Photonic spectral filter with design region area of 5.4 x 7.2 μm^2, the radius of 100 nm, and penalty radius of 100 nm : (a) Objective function error throughout optimization, (b) Penalty functions throughout optimization

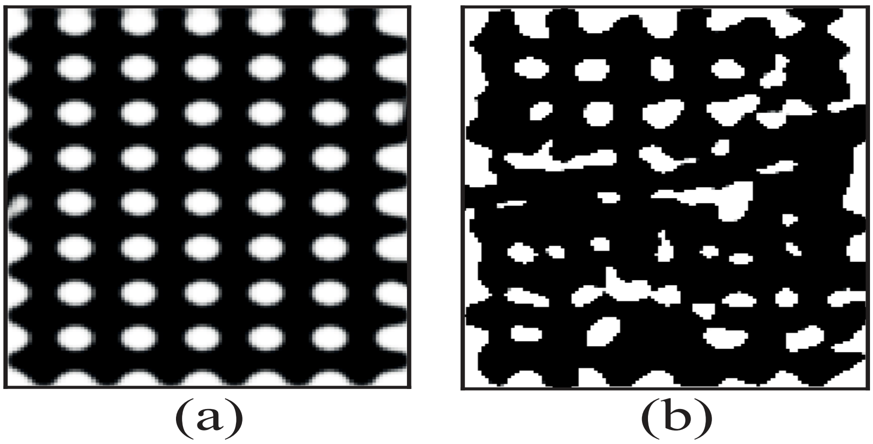

Figure 3.23: Photonic spectral filter with design region area of 5.4 x 7.2 μm^2, the radius of 100 nm, and penalty radius of 100 nm : (a) Initial guess geometry (radius of circles are 300 nm and the gap between circles is 300 nm), (b) Optimized spectral filter.

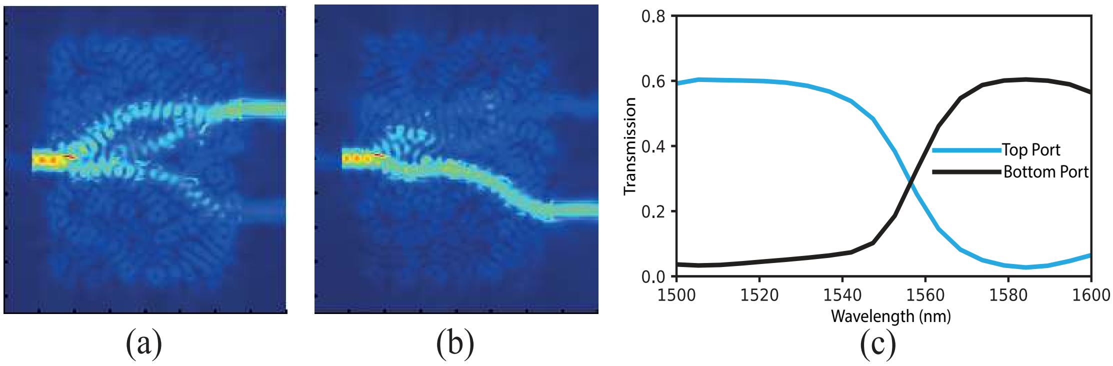

Figure 3.24: Simulation results of the photonic spectral filter shown in Figure 3.23: (a) Electric field at 1510 nm, (b) Electric field at 1590 nm, (c) 3D FDTD results.

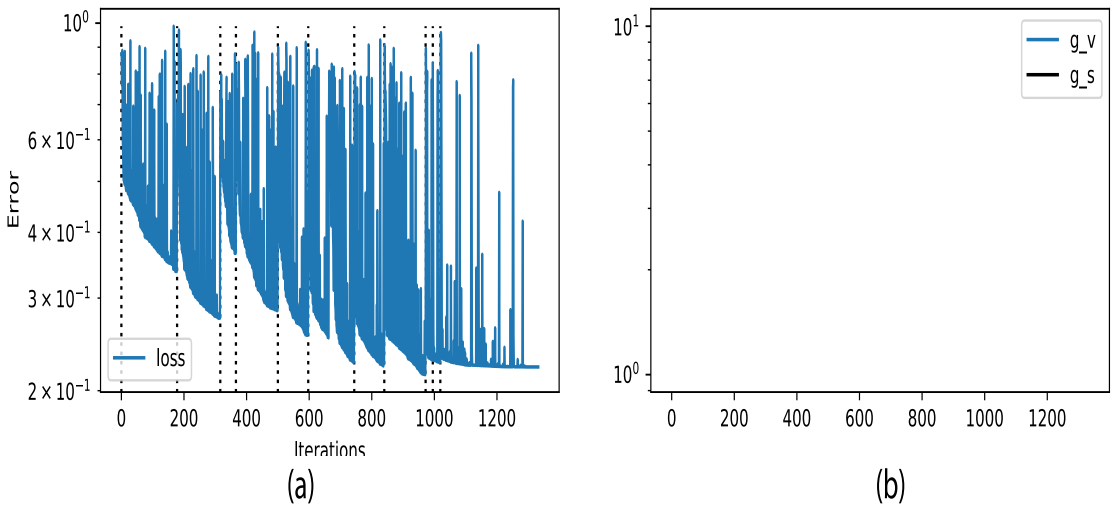

Figure 3.25: Photonic spectral filter with a design area of 6 x 7.2 µm^2, the radius and penalty radius of 250 nm : (a) Objective function error, (b) Penalty functions

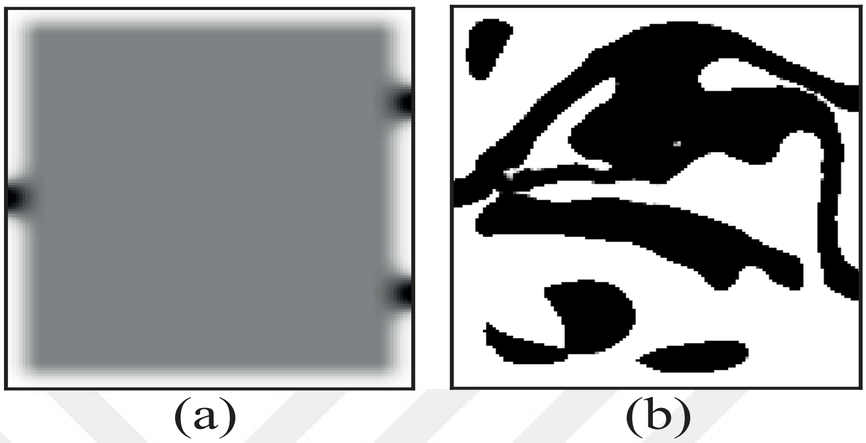

Figure 3.26: Photonic spectral filter with a design area of 6 x 7.2 µm^2, the radius and penalty radius of 250 nm : (a) Initial guess, (b) Optimized spectral filter.

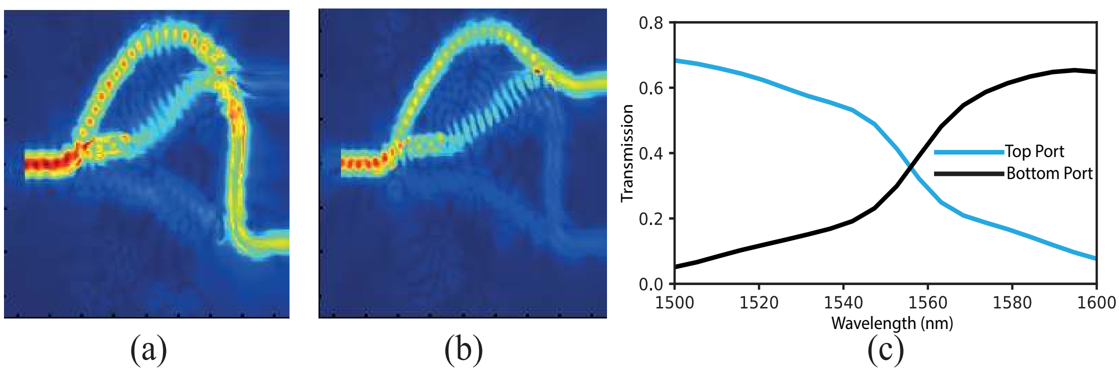

Figure 3.27: Simulation results of the photonic spectral filter shown in Figure 3.26: (a) Electric field at 1590 nm, (b) Electric field at 1510 nm, (c) 3D FDTD results.

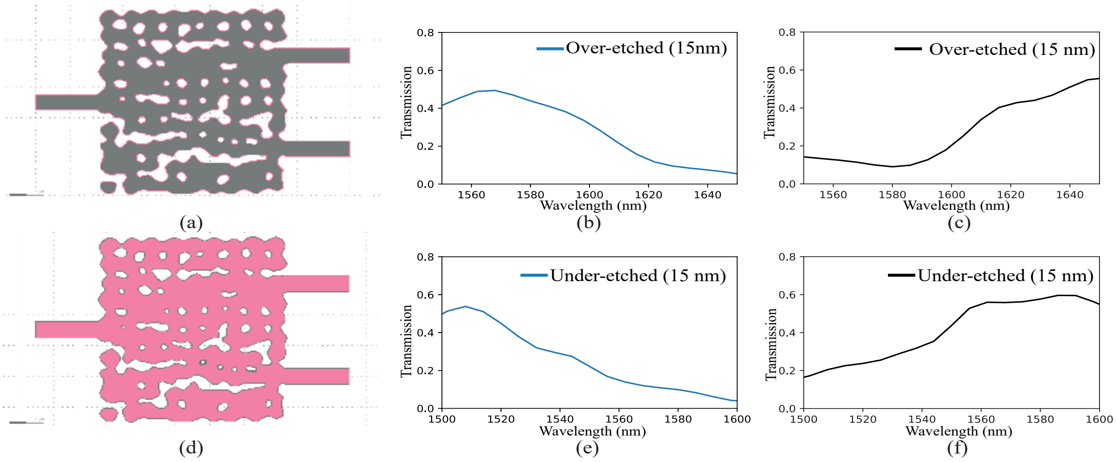

Figure 3.28: (a),(d) Over/under-etched scenarios of the device are shown in Figure 3.20b, (b),(e) 3D FDTD results at top port, (c),(f) 3D FDTD results at bottom port

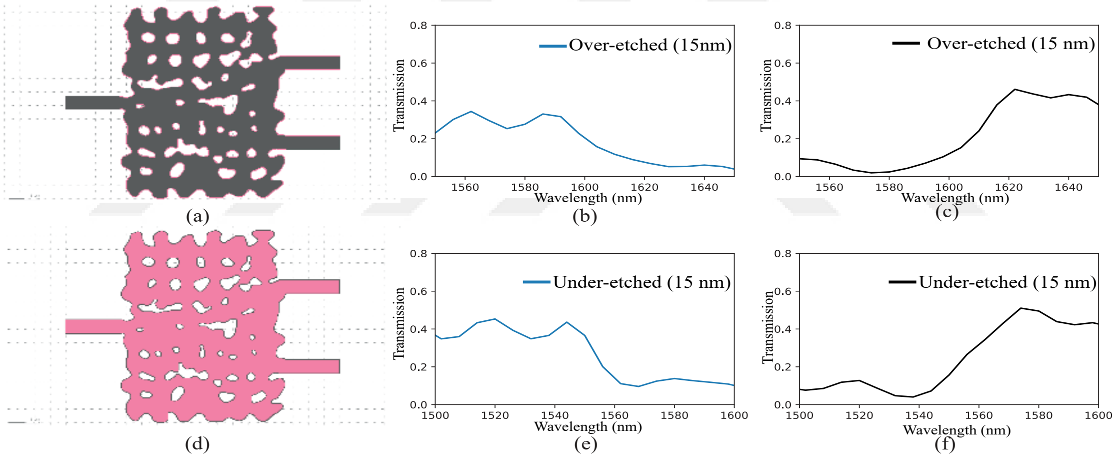

Figure 3.29: (a),(d) Over/under-etched scenarios of the device are shown in Figure 3.23b, (b),(e) 3D FDTD results at top port, (c),(f) 3D FDTD results at bottom port

Devices that are obtained using photonic crystal structure as an initial guess showed better performance. Therefore, to verify tolerance to potential fabrication changes in the geometry of the designed spectral filters that are shown in Figure 3.20b and 3.23b, over-etched (Figure 3.28a and 3.29a), and under-etched(Figure 3.28d and 3.29d) versions of the devices were simulated. Simulation results are shown above. However, these simulation results differ from optimization results. These devices are not tolerant of potential over/under etching scenarios.

Chapter 4

DEVICE FABRICATION AND EXPERIMENTAL RESULTS

The 90%:10% power splitters are fabricated in the IMECs standard passive platform and photonic spectral filters are fabricated in SiEPICfab. SOI wafers with 220 nm of silicon and silicon oxide are used.

4.1 Device Fabrication

One of the most important motivations for my work was to design fabrication-tolerant devices. The most challenging and limiting aspect of the photonic design is to achieve a photonic device design that is compatible with the fabrication requirements. Therefore, the design of fabrication-compatible photonic devices with the desired functional performances was the most important goal of my work. As described in the previous sections, different methods and operations were used to achieve a fabrication-compatible device design. And as a result, optimized devices that meet the desired and specified performance objectives and fabrication constraints are prepared for the tape-out process.

Devices are placed on a mask for the fabrication, this process is the layout process. To create a mask layout, GDS files of the photonic devices are obtained. To extract GDS patterns of the designed devices, the Lumerical GDS extraction method, Gdspy, and Gdstk are used as tools. To view and edit the GDS patterns of devices, KLayout is used.

Before the photonic devices are placed in the mask, the consistency of the 3D FDTD simulation results of the GDS patterns and whether the devices fully satisfied the fabrication constraints are checked.

After creating the GDS files, 3D FDTD simulations of the photonic devices are performed by importing the GDS files of the devices and compared with the simulation results of the actual devices. Because during extraction of the GDS pattern of devices, there may be small changes in the device geometry. GDS patterns with 3D FDTD simulation results matching the 3D FDTD simulation results of the optimized device were used for fabrication.

```
report("Dimension and Angle Check")

wg_cor = input(1,0)
wg_cor.width(150.nm).output("WG.W.150", "min WG width=0.15")
wg_cor.drc(130.nm <= width < 150.nm).output("WARNING.WG.W.150", "WG width < 0.15 and >= 0.13 allowed but out of process window")

wg_cor.space(150.nm).output("WG.S.150", "min WG spacing=0.15")
wg_cor.drc(130.nm <= space < 150.nm).output("WARNING.WG.S.150", "WG spacing < 0.15 and >= 0.13 allowed but out of process window")
wg_cor.corners(95 .. 180, -180 .. -95).output("WG.SHARPANGLE", "Angle < 85 degrees")

fc_cor = input(37,4)
fc_cor.width(150.nm).output("FC.W.150", "min FC width=0.15")
fc_cor.space(150.nm).output("FC.S.150", "min FC spacing=0.15")
fc_cor.corners(95 .. 180, -180 .. -95).output("FC.SHARPANGLE", "Angle < 85 degrees")

skt_cor = input(37,4)
skt_cor.width(130.nm).output("SKT.W.130", "min SKT width=0.13")
skt_cor.space(130.nm).output("SKT.S.130", "min SKT spacing=0.13")
skt_cor.corners(95 .. 180, -180 .. -95).output("SKT.SHARPANGLE", "Angle < 85 degrees")
```

Listing 4.1: DRC script

Despite the many different filtering and penalty methods used during inverse design optimization, it is quite hard to achieve a fully fabrication-compatible device design. Because the optimization performs based on many design and functional performance constraints. Therefore, devices were checked if they are fabrication-compatible or not, before mask layout. This process is called DRC. DRC of the devices is performed using their GDS patterns and KLayout. The script shown in Listing 4.1 is used for DRC.

There are different fabrication limitations due to the materials, techniques, and tools used for fabrication. In the DRC code in Listing 4.1, different DRC checks are performed by changing the minimum feature size and sharp angle values depending on the requirements and limitations of fabrication. The features of the devices are not compatible with fabrication, so DRC errors are detected as shown in Figure 4.1. Figure 4.1a shows the DRC errors and their reasons and categories and Figure 4.1b shows where each DRC error is located in the device geometry. Furthermore, Figure 4.1a also shows warnings of minimum features that have no DRC error but are close to fabrication limitations.

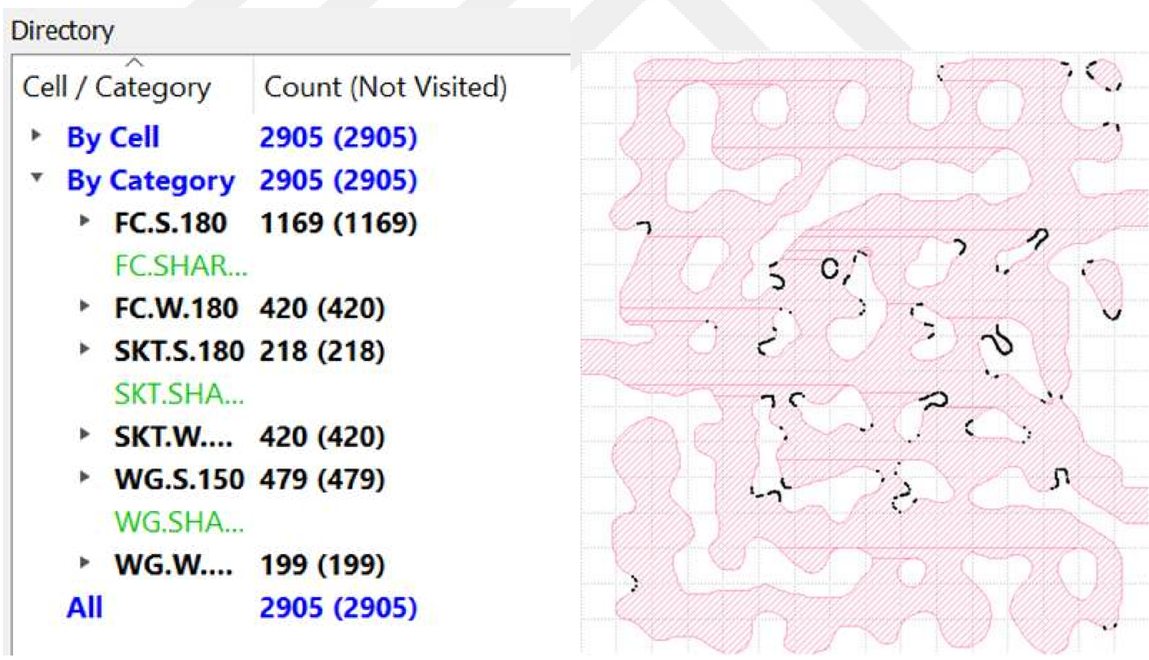

(a) (b)

Figure 4.1: Design Rule Checking Operation (a) DRC categories, (b) DRC errors on device geometry.

After DRC control, device geometries are edited to make devices ready for tape-out. To see if there is a change in the performance of the modified devices, 3D FDTD simulations were made and compared with the original devices' performance results. Modifications on device geometries are performed in KLayout, and 3D FDTD simulations of GDS patterns of the devices are performed in Lumerical.

In the following sections, the GDS pattern extraction methods and tools, DRC, layout, and 3D FDTD simulations of the photonic power splitter and photonic spectral filters are analyzed and explained.

4.1.1 90%:10% Power Splitter

To extract the GDS of splitters, the contours method that Lumerical proposes [Lumerical, 2022a] is used. The contours method creates GDS using index data from the simulation. This method determines exactly where each point will fall depending on the threshold and index values. For different threshold values, different GDS patterns for the device are obtained. There are small differences between these GDS patterns for the same device. And, these minor differences cause discrepancies in simulation results. Therefore, different GDS patterns were obtained using different threshold values for the same power splitter and 3D FDTD simulations were performed and compared in the following Figures 4.2 and 4.3.

The graphs below show the 3D FDTD simulation results of the GDS shapes obtained with different threshold values of the designed devices and these results are compared with the simulation results of the designed device. The simulation results for both output ports are very comparable to each other and to the transmission results of the optimized device and are quite similar to the target FOM.

Then, based on comparisons, the best-performing GDS pattern matches well with the optimization results, and the design targets are selected for fabrication and edited according to fabrication constraints.

GDS patterns of 3D optimized power splitters, their DRC results, and modified GDS patterns according to DRC are shown in Figures 4.4 and 4.5. Figures 4.4a and 4.5a show the optimized device geometries, Figures 4.4b and 4.5b show the DRC errors on devices, and Figures 4.4c and 4.5c show modified geometries after DRC.

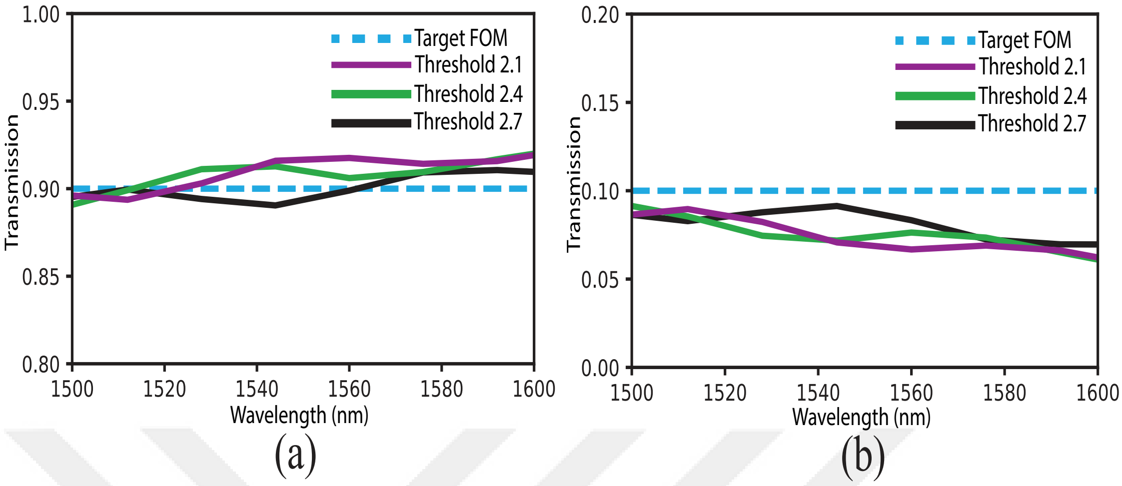

Figure 4.2: Simulation results of GDS files of 90%:10% power splitter shown in Figure 3.9 (a) 3D FDTD simulation results of the top port, (b) 3D FDTD simulation results of the bottom port.

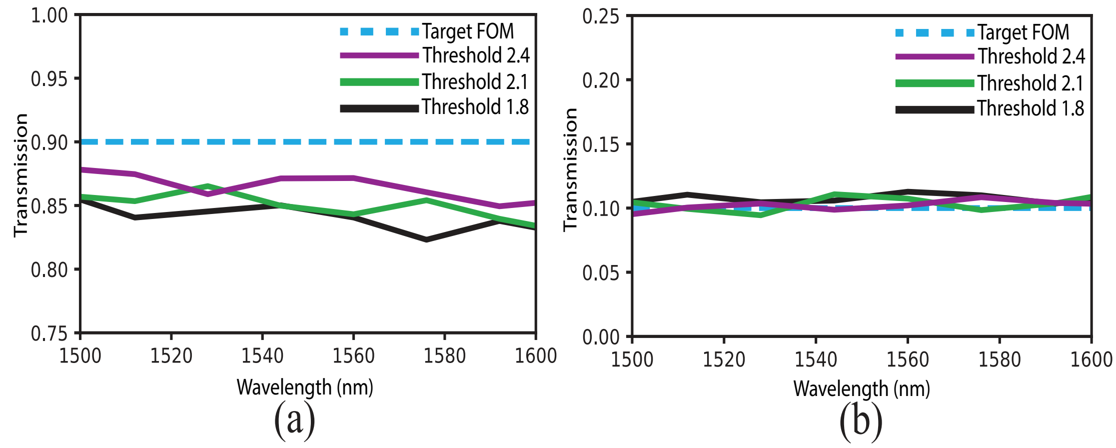

Figure 4.3: Simulation results of GDS files of 90%:10% Y-Splitter shown in Figure 3.14 (a) 3D FDTD simulation results of the top port, (b) 3D FDTD simulation results of the bottom port.

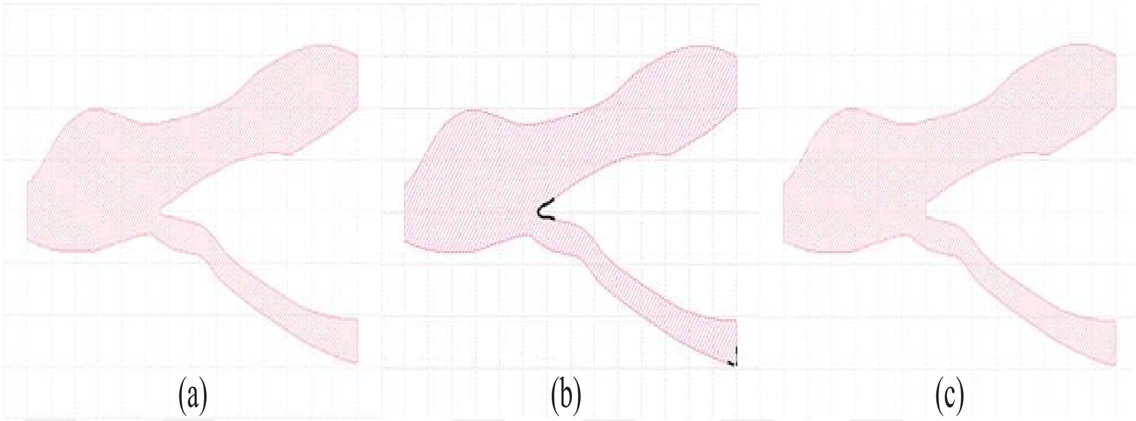

Figure 4.4: GDS patterns of 90%:10% power splitter shown in Figure 3.9 (a) GDS pattern of the original power splitter, (b) DRC results, (c) GDS pattern of the modified power splitter.

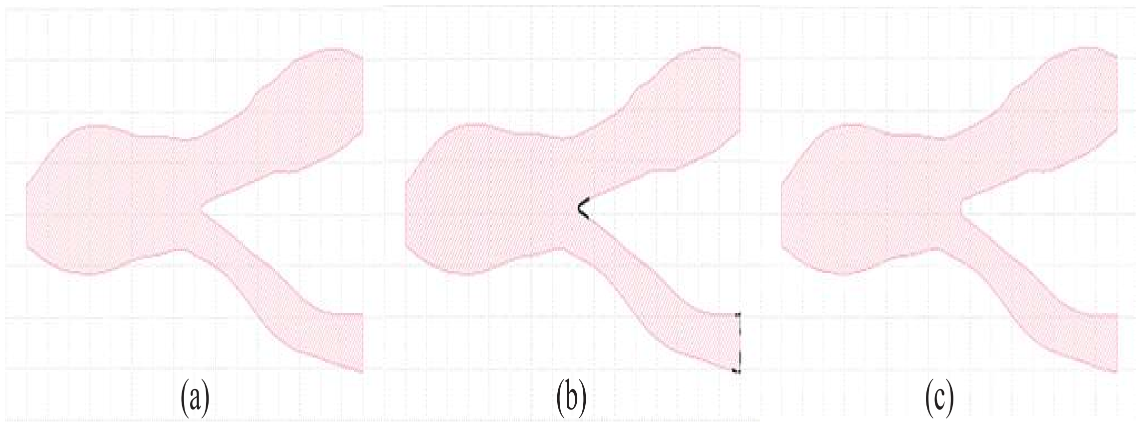

Figure 4.5: GDS patterns of 90%:10% power splitter shown in Figure 3.14 (a) GDS pattern of the original power splitter, (b) DRC results, (c) GDS pattern of the modified power splitter.

The device geometries in Figure 4.4c and Figure 4.5c are placed on the mask(layout) and tape-out. Their measurement results are presented in the next section.

4.1.2 Photonic Spectral Filter

Gdstk (GDSII Tool Kit) was used to obtain the GDS formats of the designed filters. Gdstk is an open-source library for creating and editing GDS. The details of the GDS extraction are presented below:

1. In our optimization model, the device geometry is saved as a 2D array. Contour points are extracted from this black-and-white 2D array. To reduce the conversion error, we first upscale the array.

2. By finding the B-spline representation, contour curves are smoothed.

3. Finally, the black-and-white 2D array with information on the device geometry is converted to a GDSII file.

GDS patterns of 3D optimized photonic spectral filters, their DRC results, and modified GDS patterns of them after DRC are shown in Figures 4.6 and 4.8.

The photonic spectral filters obtained have more complex geometric structures (Figures 4.6 and 4.8) than power splitters, and therefore have more features in small dimensions. Therefore, more DRC errors occur. Correcting these errors requires more attention and time. Considering the optimization time, complex geometrical structure, and functionalities, filter design is more challenging.

After DRC, modifications were made in the device geometries and the modified GDS files were imported to Lumerical and 3D FDTD simulations were performed in Lumerical. However, the simulations of the optimized photonic spectral filters were performed with Meep. There are differences between the transmission results due to possible material index differences or similar differences between the two tools Meep and Lumerical. In addition, since the filters have complex geometric structures, their geometry has been further modified, which may cause more significant differences in the transmission results. Comparing the two simulation results, there is a shift in wavelengths. Figure 4.7 and 4.9 shows the 3D FDTD simulation results of the modified spectral filters shown in Figure 4.6c and 4.8c respectively. This difference is also seen in the measurement results.

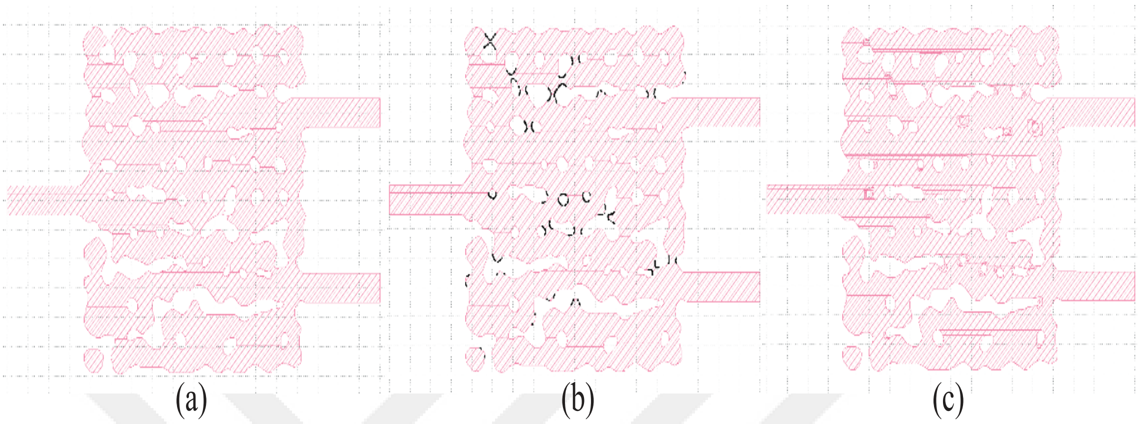

Figure 4.6: GDS patterns of the photonic spectral filter shown in Figure 3.19 (a) GDS pattern of the original filter, (b) DRC results, (c)The modified filter's GDS.

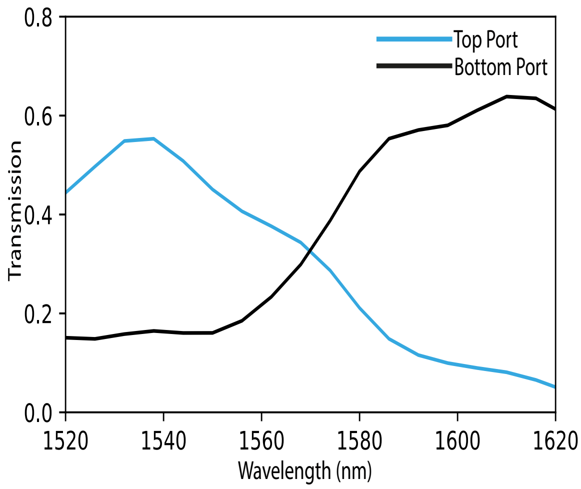

Figure 4.7: Simulation results of the edited photonic spectral filter shown in Figure 4.6c

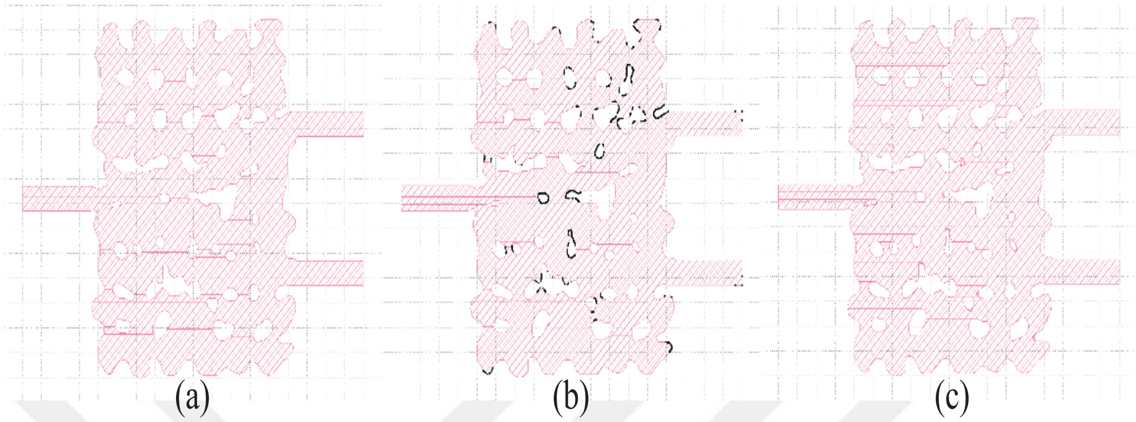

Figure 4.8: GDS patterns of the photonic spectral filter shown in Figure 3.22 (a) GDS pattern of the original filter, (b) DRC results, (c)The modified filter's GDS.

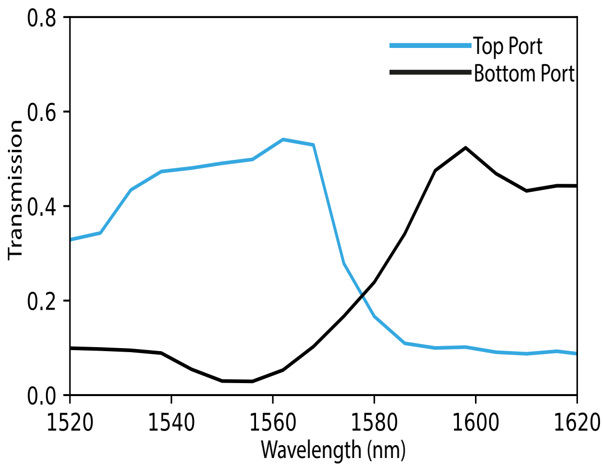

Figure 4.9: Simulation results of the edited photonic spectral filter shown in Figure 4.8c

The camera image of the chip where the photonic spectral filters are placed is given in Figure 4.10.

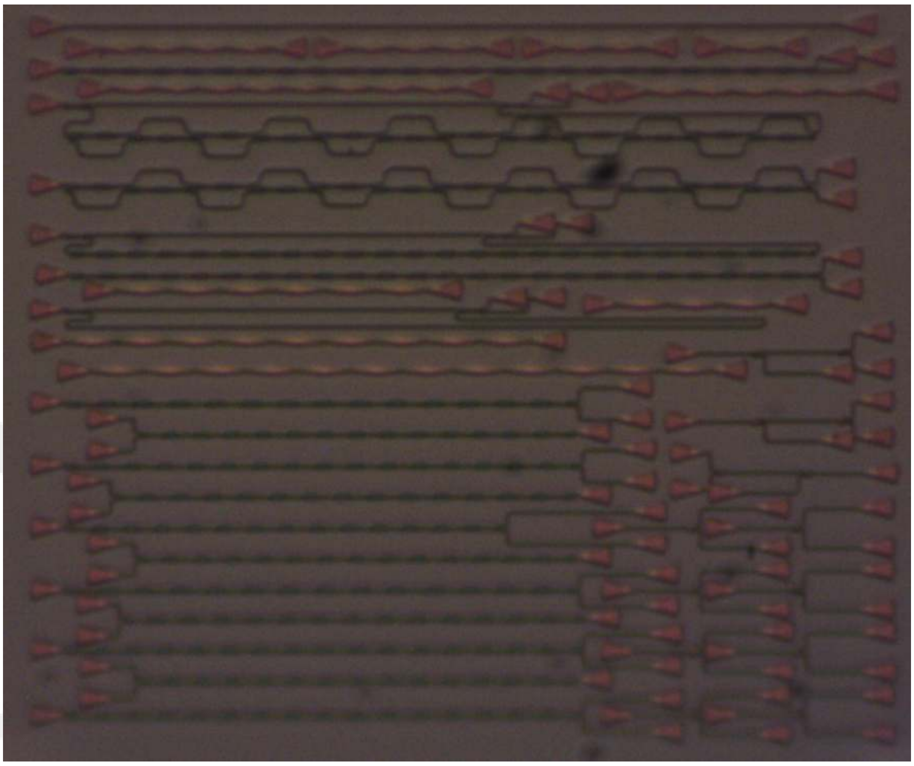

Figure 4.10: Camera image of the chip photonic spectral filters are placed

4.2 Experimental Results

The measurements of the devices are performed with a tunable laser between 1480 and 1640 nm wavelengths. To obtain the transmission results and spectrum of the devices, the spectrum of the fiber grating couplers at the input and output ports of the devices are subtracted from the measurement results. Transmission measurements of fiber grating couplers were performed with fiber grating couplers located at the input and output ends of a straight waveguide.

The setup for the measurement of the devices is shown in Figure 4.11 below.

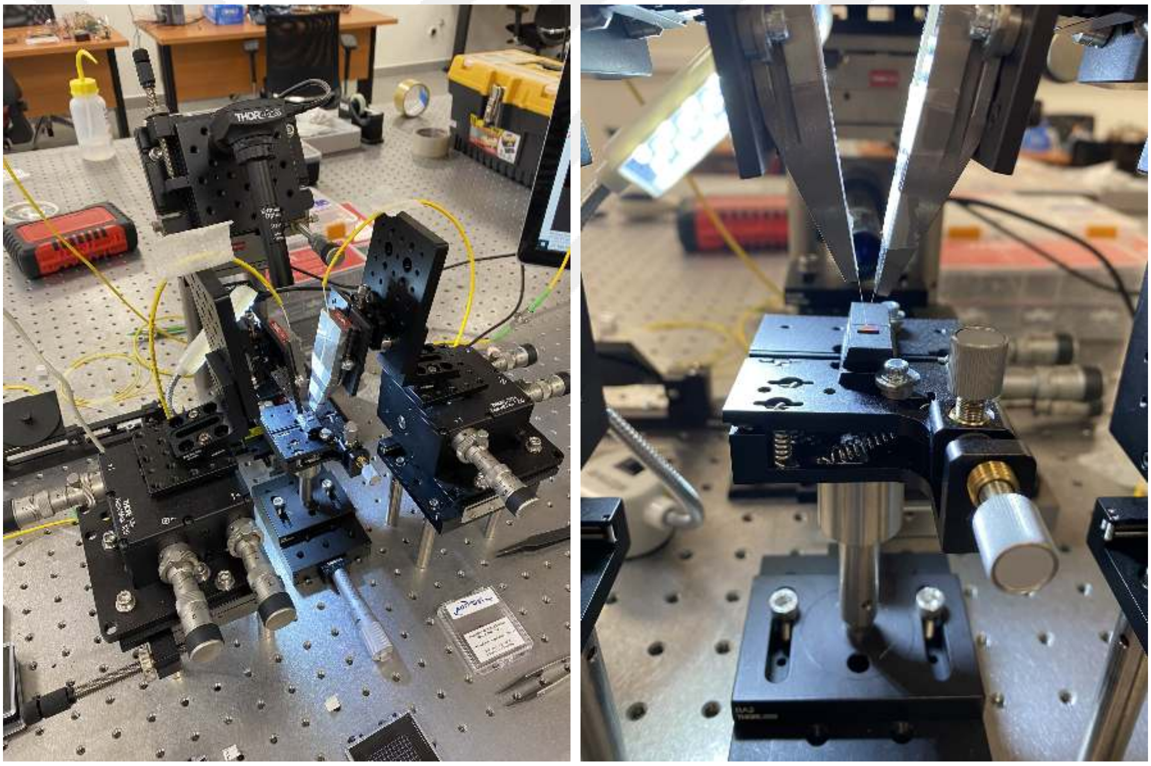

(a) (b)

Figure 4.11: Measurement setup

The chip shown in Figure 4.11b is the chip where the photonic power splitters are placed and the image was captured during the measurement of the power splitters.

4.2.1 90%:10% Power Splitter

As shown in Figures 4.12 and 4.13 below, the power splitters achieve state-of-the-art performance with very low excess losses and broadband operation. The experimental results match closely with the user-specified figure of merit throughout the 1500-1600 nm range. The output ports of the power splitters perform wide-band flatness.

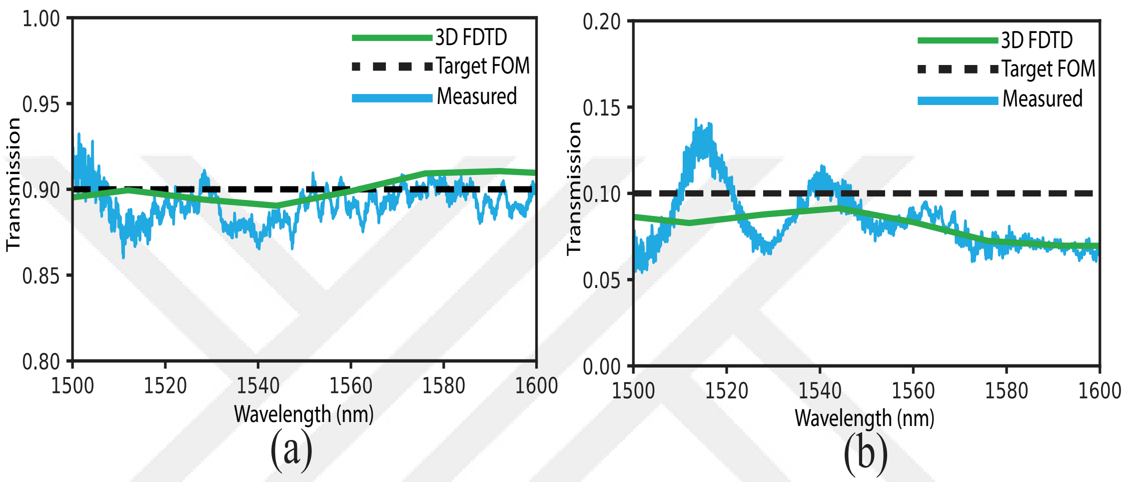

Figure 4.12: Measured and simulated transmission results of 90%:10% power splitter shown in Figure 3.9 (a) Transmission results of the top port, (b) Transmission results of the bottom port.

The excess loss recorded reaches a maximum of only 0.23 dB and 1.37 dB for 90%:10% power splitters respectively, demonstrating the high performance of the fabricated device. These measurement results confirm both the fabrication compatibility of the device, as well as its potential tolerance to possible over-etch and under-etch scenarios during the fabrication process.

Simulation and measurement results show that a 90%:10% power splitter with a design region area of 7.0 x 7.0 μm^2 achieves better performance and its performance matches very well with the design performance targets. However, both devices perform quite successfully and are in a similarity to the simulation results.

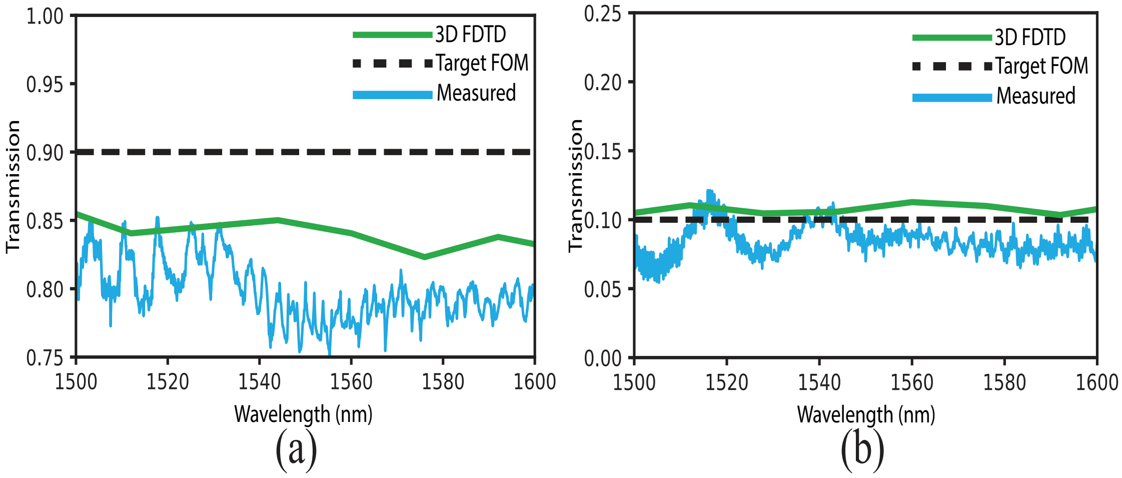

Figure 4.13: Measured and simulated transmission results of 90%:10% power splitter shown in Figure 3.14 (a) Transmission results of the top port, (b) Transmission results of the bottom port.

4.2.2 Photonic Spectral Filter

The measurement results of the photonic filters are shown in the figures below. Figure 4.14 shows the measurement results of the optimized filter presented in Figure 3.19b and Figure 4.15 shows the measurement results of the optimized filter presented in Figure 3.22b. There are non-negligible differences between simulation results and measurement results. There is a shift in wavelengths, but the spectral response of the filter is not completely observed. This is because the wavelength range of the laser used during the measurement process is between 1480-1640nm and this wavelength range is not enough to see the response of the filters.

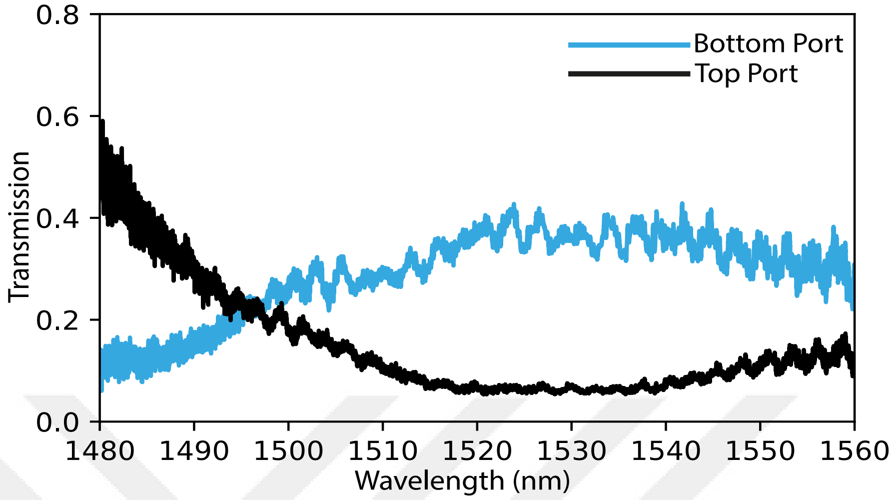

Figure 4.14: Measured transmission results of the photonic spectral filter shown in Figure 3.19

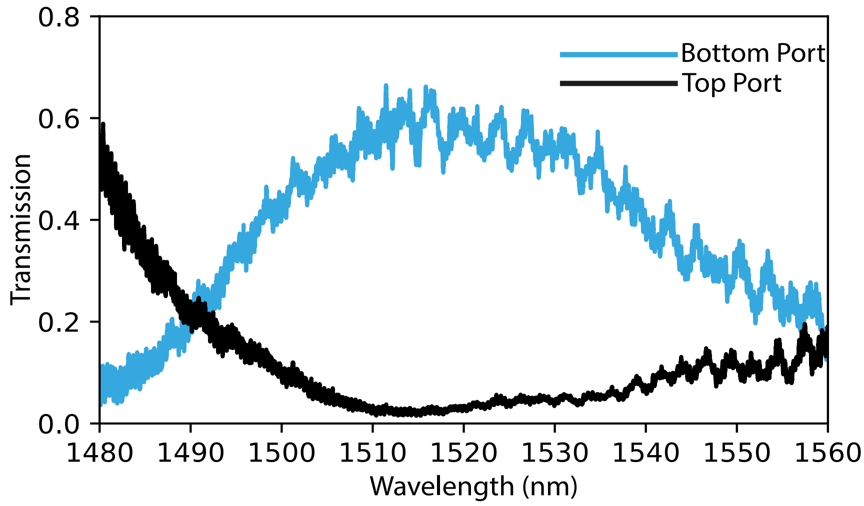

Figure 4.15: Measured transmission results of the photonic spectral filter shown in Figure 3.22

Chapter 5

CONCLUSION

This thesis describes the design and optimization of various fabrication-compatible photonic devices with different functional properties using the inverse design method. Photonic inverse design is finding the geometrical structures of photonic devices by defining design variables, such as size, material, and initial guess, and performance specifications, like power splitting, mode converter, and wavelength filtering. At the end of the optimization, the devices meet these defined specifications. The inverse design of photonic devices is quite challenging, and the computational cost is high. An adjoint-based topology optimization was used in the inverse design of photonic devices. Using an adjoint-based topology optimization method for photonic inverse design decreases the computational cost of the optimization and enables the design of photonic devices that can perform highly efficiently. Although the devices designed with the topology optimization method perform with low losses, they can be in geometric structures with small-size features that are not compatible with fabrication. To overcome this drawback of the topology optimization method, various filtering techniques were used during optimization to make the devices fabrication-compatible. In the design process of photonic devices, electromagnetic simulations were performed with FDTD. The inverse design was performed with both 2D and 3D FDTD simulations. Although simple photonic devices were obtained in a very short time with 2D FDTD simulations, more accurate results were obtained with 3D FDTD simulations, so the studies were continued with 3D simulations.

Using the inverse design method photonic power splitter and spectral filter were designed and fabricated. The design process, tools and methods, optimization and simulation results of these photonic devices, their layout and tape-out processes like GDS extraction, and DRC, and measurement results of fabricated devices are explained in detail in previous chapters.

90%:10% power splitters are designed in the Lumerical using the inverse design method for TE-polarized light. And fabricated in the IMECs platform. SOI wafers with 220 nm of silicon and buried oxide are used. 90%:10% power splitter design was performed in Lumerical with 2D and 3D FDTD simulations. Lumerical makes the photonic devices fabrication-compatible by minimizing small features and smoothing sharp corners and angles of the device geometry throughout the optimization using a filter whose radius is determined by the user. The power splitters with 2D simulations showed very good performance and fabrication compatibility. However, when 3D FDTD simulations of these devices were performed, there was a difference between the 2D simulations. For this reason, they were inverse-designed with 3D FDTD. The performance results and fabrication compatibility of the 3D-optimized devices were found to be more successful than the 2D-optimized devices, as expected, and they have fabricated after small modifications on the device geometries due to DRC. The simulation results and measurement results of the photonic 90%:10% power splitter match. The inverse design of the photonic spectral filters was performed with 3D FDTD simulations in Meep for TE-polarized light. And fabricated in the SiEPICfab platform. SOI wafers with 220 nm of silicon and silicon oxide are used. Since spectral filters are more complex structures than power splitters, their inverse design optimization has a higher computational cost. And gradient calculations in Meep are faster than in Lumerical. Therefore, to design a photonic spectral filter Meep is used as a tool. Also, to obtain more accurate results 3D FDTD simulations were performed instead of 2D simulations. In the optimization of photonic spectral filters, smoothing, filtering, projection, opening, and closing operations were used to make them compatible with fabrication. The geometry of filters with complex geometric structures has been further modified after DRC. Measurement and simulation results of the fabricated photonic spectral filters are quite different from each other. However, due to the wavelength range of the laser used in the measurement, the exact response of the spectral filters could not be determined. The reason for these differences may be that the wavelength-dependent material index is defined in Meep only according to the center wavelength.

All in all, it has been obtained low-loss, broadband, and fabrication-compatible photonic devices by using the inverse design method in the design of photonic devices. More robust and successful results can be achieved by defining more design variables or specifying these variables in more detail in the design of photonic devices with complex functionalities. Also, new optimization approaches and algorithms can be developed in the next step of the project to improve the fabrication compatibility of photonic devices with complex structures. Furthermore, the measurement results can be matched with simulation results by defining the values of the material indices for each wavelength separately.

BIBLIOGRAPHY

[Angeris et al., 2021] Angeris, G., Vučković, J., and Boyd, S. (2021). Heuristic methods and performance bounds for photonic design. *Opt. Express*, 29(2):2827–2854.

[Chang et al., 2018] Chang, W., Ren, X., Ao, Y., Lu, L., Cheng, M., Deng, L., Liu, D., and Zhang, M. (2018). Inverse design and demonstration of an ultracompact broadband dual-mode 3 db power splitter. *Opt. Express*, 26(18):24135–24144.

[Christiansen et al., 2015] Christiansen, R. E., Lazarov, B. S., Jensen, J. S., and Sigmund, O. (2015). Creating geometrically robust designs for highly sensitive problems using topology optimization. *Structural and Multidisciplinary Optimization*, 52(4):737–754.

[Christiansen and Sigmund, 2021] Christiansen, R. E. and Sigmund, O. (2021). Inverse design in photonics by topology optimization: tutorial. *Journal of the Optical Society of America B*, 38(2):496–509.

[Christopher Lalau-Keraly, 2022] Christopher Lalau-Keraly (accessed 2022). Continuous adjoint optimization wrapper for lumerical. `https://github.com/chriskeraly/lumopt.git`.

[Dasdemir et al., 2020] Dasdemir, A. O., Koral, A. K., Kiraz, B., Kiraz, A., and Magden, E. S. (2020). Multi-scale hierarchical topology optimization for nanophotonic design. In *OSA Advanced Photonics Congress (AP) 2020 (IPR, NP, NOMA, Networks, PVLED, PSC, SPPCom, SOF)*, page ITu4A.11. Optica Publishing Group.

[Eichenfield et al., 2009] Eichenfield, M., Chan, J., Camacho, R. M., Vahala, K. J., and Painter, O. (2009). Optomechanical crystals. *Nature*, 462(7269):78–82.

[Hammer and Ivanova, 2009] Hammer, M. and Ivanova, O. (2009). Effective index approximations of photonic crystal slabs: A 2-to-1-d assessment. *Optical and Quantum Electronics*, 41:267–283.

[Hammond et al., 2022] Hammond, A. M., Oskooi, A., Chen, M., Lin, Z., Johnson, S. G., and Ralph, S. E. (2022). High-performance hybrid time/frequency-domain topology optimization for large-scale photonics inverse design. *Opt. Express*, 30(3):4467–4491.

[Jalali and Fathpour, 2006] Jalali, B. and Fathpour, S. (2006). Silicon photonics. *Journal of Lightwave Technology*, 24(12):4600–4615.

[Jensen and Sigmund, 2011] Jensen, J. S. and Sigmund, O. (2011). Topology optimization for nano-photonics. *Laser Photonics Reviews*, 5(2):308–321.

[Kalyani and Sharma, 2016] Kalyani, V. and Sharma, V. (2016). Different types of optical filters and their realistic application. *Journal of Management Engineering and Information Technology*, 3.

[Lalau-Keraly et al., 2013] Lalau-Keraly, C. M., Bhargava, S., Miller, O. D., and Yablonovitch, E. (2013). Adjoint shape optimization applied to electromagnetic design. *Opt. Express*, 21(18):21693–21701.

[Liu et al., 2020] Liu, Y., Yao, Y., Du, J., and Xu, K. (2020). Inverse design of integrated four-channel mode multiplexer with dual polarizations. In *Asia Communications and Photonics Conference/International Conference on Information Photonics and Optical Communications 2020 (ACP/IPOC)*, page M4A.131. Optica Publishing Group.

[Lumerical, 2022a] Lumerical (accessed 2022a). Gds pattern extraction for inverse designed devices using contours method. `https://optics.ansys.com/hc/en-us/articles/1500007228522-GDS-pattern-extraction-for-inverse-designed-devices-using-contou`

[Lumerical, 2022b] Lumerical (accessed 2022b). Lumerical. `https://www.lumerical.com/`.

[Lumerical, 2022c] Lumerical (accessed 2022c). Lumerical's 2.5d fdtd propagation method. `https://www.lumerical.com/learn/whitepapers/lumericals-2-5d-fdtd-propagation-method/`.

[MEEP, 2022] MEEP (accessed 2022). Meep documentation. `https://meep.readthedocs.io/en/latest/`.

[Miller, 2012] Miller, O. D. (2012). *Photonic Design: From Fundamental Solar Cell Physics to Computational Inverse Design*. PhD thesis, University of California, Berkeley.

[OPTICA, 2022] OPTICA (accessed 2022). Inverse design methods for novel, high-performance and manufacturable components for photonic integrated circuits. `https://www.optica.org/en-us/events/webinar/2020/february/inverse_design_methods_for_novel_high-performance/`.

[Piggott et al., 2016] Piggott, A. Y., Lu, J., Lagoudakis, K. G., Petykiewicz, J., Babinec, T. M., and Vučković, J. (2016). Inverse design of a wavelength demultiplexer. In *2016 Conference on Lasers and Electro-Optics (CLEO)*, pages 1–2.

[Sanchis et al., 2009] Sanchis, P., Villalba, P., Cuesta, F., Håkansson, A., Griol, A., Galán, J. V., Brimont, A., and Martí, J. (2009). Highly efficient crossing structure for silicon-on-insulator waveguides. *Opt. Lett.*, 34(18):2760–2762.

[Wong et al., 2007] Wong, H., Filip, V., Wong, C., and Chung, P. (2007). Silicon integrated photonics begins to revolutionize. *Microelectronics Reliability*, 47(1):1–10.

[Xu et al., 2022] Xu, J., Liu, Y., Guo, X., Song, Q., and Xu, K. (2022). Inverse design of a dual-mode 3-db optical power splitter with a 445 nm bandwidth. *Opt. Express*, 30(15):26266–26274.

[Xu et al., 2008] Xu, Q., Fattal, D., and Beausoleil, R. G. (2008). Silicon microring resonators with 1.5-µm radius. *Opt. Express*, 16(6):4309–4315.

[Yeung et al., 2022] Yeung, C., David Ho, B. P., Fountaine, K. T., Zhang, Z., Levy, K., , and Raman, A. P. (2022). Enhancing adjoint optimization-based photonic inverse design with explainable machine learning. *ACS Photonics*, 9(5):1577–1585.

[Yin, 2019] Yin, G. (2019). Photonic inverse design for 3-d structures and optical phase change materials. Master's thesis, Massachusetts Institute of Technology.

[Zhang et al., 2013] Zhang, Y., Yang, S., Lim, A. E.-J., Lo, G.-Q., Galland, C., Baehr-Jones, T., and Hochberg, M. (2013). A compact and low loss y-junction for submicron silicon waveguide. *Opt. Express*, 21(1):1310–1316.

[Zhou et al., 2015] Zhou, M., Lazarov, B. S., Wang, F., and Sigmund, O. (2015). Minimum length scale in topology optimization by geometric constraints. *Computer Methods in Applied Mechanics and Engineering*, 293:266–282.

[Zhu et al., 1997] Zhu, C., Byrd, R. H., Lu, P., and Nocedal, J. (1997). Algorithm 778: L-bfgs-b: Fortran subroutines for large-scale bound-constrained optimization. *ACM Trans. Math. Softw.*, 23(4):550–560.